Neurobiology of Disease

Delayed Postnatal Loss of P/Q-Type Calcium Channels Recapitulates the Absence Epilepsy, Dyskinesia, and Ataxia Phenotypes of Genomic *Cacna1A* Mutations

Melanie D. Mark,[1] Takashi Maejima,[1] Denise Kuckelsberg,[1] Jong W. Yoo,[3] Robert A. Hyde,[2] Viral Shah,[2] Davina Gutierrez,[2] Rosa L. Moreno,[4] Wolfgang Kruse,[1] Jeffrey L. Noebels,[3] and Stefan Herlitze[1,2]

[1]Department of Zoology and Neurobiology, ND7/31, Ruhr-University Bochum, D-44780 Bochum, Germany, [2]Department of Neurosciences, Case Western Reserve University, Cleveland, Ohio 44106-4975, [3]Department of Neurology, Baylor College of Medicine, Houston, Texas 77030, and [4]Department of Physiology and Biophysics, University of Colorado (Anschutz Medical Campus), Aurora, Colorado 80045

Inherited loss of P/Q-type calcium channel function causes human absence epilepsy, episodic dyskinesia, and ataxia, but the molecular "birthdate" of the neurological syndrome and its dependence on prenatal pathophysiology is unknown. Since these channels mediate transmitter release at synapses throughout the brain and are expressed early in embryonic development, delineating the critical circuitry and onset underlying each of the emergent phenotypes requires targeted control of gene expression. To visualize P/Q-type Ca^{2+} channels and dissect their role in neuronal networks at distinct developmental stages, we created a novel conditional *Cacna1a* knock-in mouse by inserting the floxed green fluorescent protein derivative Citrine into the first exon of *Cacna1a* and then crossed it with a postnatally expressing PCP2-Cre line for delayed Purkinje cell (PC) gene deletion within the cerebellum and sparsely in forebrain (*purky*). PCs in *purky* mice lacked P/Q-type calcium channel protein and currents within the first month after birth, displayed altered spontaneous firing, and showed impaired neurotransmission. Unexpectedly, adult *purky* mice exhibited the full spectrum of neurological deficits seen in mice with genomic *Cacna1a* ablation. Our results show that the ataxia, dyskinesia, and absence epilepsy caused by inherited disorders of the P/Q-type channel arise from signaling defects beginning in late infancy, revealing an early window of opportunity for therapeutic intervention.

Introduction

Voltage-gated Ca^{2+} channels (VGCCs) including P/Q-type channels regulate integrative signaling and synaptic output in most CNS neurons (Reid et al., 2003). P/Q-type channels were first identified in cerebellar Purkinje cells (PCs) (Llinas et al., 1989; Mintz et al., 1992a) and consist of a protein complex of pore-forming Cacna1A and auxiliary subunits (Catterall, 2000). In PCs, somatodendritic P/Q-type channels are a major source of Ca^{2+} transients and contribute to the firing and waveform of action potentials (Womack and Khodakhah, 2004; Hartmann and Konnerth, 2005). At presynaptic sites, P/Q-type channels trigger the vesicular release of neurotransmitter (Dunlap et al., 1995; Catterall and Few, 2008).

P/Q-type channels share the release function with other Ca^{2+} channels, including N and R type, with variable contributions to evoked transmitter release during development (e.g., early postnatal transmitter release can rely on a high contribution of N-type channels followed by a P/Q-type dominance in the second postnatal week), whereas at other synapses, N-type release remains dominant (Iwasaki et al., 2000).

Various inherited and targeted mutations of *Cacna1a* and auxiliary subunit genes that cause ataxia have been identified in humans and mice, as first described in the *tottering* mutant and its alleles (Fletcher et al., 1996; Burgess and Noebels, 1999; Mori et al., 2000; Zwingman et al., 2001). Human ataxic phenotypes with cerebellar atrophy include SCA6 and EA2 (Kordasiewicz and Gomez, 2007; Strupp et al., 2007). Mouse models show varying degrees of cerebellar pathology, from minimal dendritic atrophy and PC loss in *tottering* to more severe dystrophy in other alleles (Fletcher et al., 1996; Burgess and Noebels, 1999; Mori et al., 2000; Zwingman et al., 2001; Kodama et al., 2006; Sawada et al., 2009; Pietrobon, 2010). Mutations in the auxiliary subunits *Cacnb4* (*lethargic*) and *Cacna2d2* (*ducky*) and targeted *Cacna1a*-deficient mutants also show similar mild atrophic pathology (Fletcher and Frankel, 1999; Jun et al., 1999; Barclay et al., 2001; Fletcher et al., 2001; Brodbeck et al., 2002). Along with the cerebellar atrophy and associated ataxia, *Cacna1a* mutations produce seemingly unrelated paroxysmal phenotypes appearing at distinct developmental stages (Pietrobon, 2010). Absence seizures arising from aberrant oscillations in synaptically linked neocortex and reticular and thalamic relay circuits in mouse models

Received Oct. 12, 2010; revised Jan. 12, 2011; accepted Jan. 20, 2011.

This work was supported by National Institutes of Health Grants NS29709, HD024064 (J.L.N.), Deutsche Forschungsgemeinschaft HE2471/8-1, and MH081127 (S.H.); Japan Society for the Promotion of Science Postdoctoral Fellowships for Research Abroad (T.M.), and Grant R36MH086283 (D.G.). We thank Drs. E. S. Deneris, D. D. Friel, and L. T. Landmesser for reading this manuscript; Dr. Stephen O'Gorman for his guidance in designing the targeting vector; Dr. Ron Conlon and the Case Transgenic and Targeting Facility for creating the mice; and Dr. Gemma Casadesus and the Case Western Reserve University Rodent Behavior Core for assistance in the behavior studies. We also thank Stephanie Krämer, Margareta Möllmann, Manuela Schmidt, Winfried Junke, Hermann Korbmacher, and Volker Rostek for excellent technical assistance.

Correspondence should be addressed to Stefan Herlitze, Department of Zoology and Neurobiology, ND7/31, Ruhr-University Bochum, Universitätsstrasse 150, D-44780 Bochum, Germany. E-mail: Stefan.Herlitze@rub.de.

DOI:10.1523/JNEUROSCI.5342-10.2011

 0270-6474/11/314311-16$15.00/0

appear as early as postnatal day 13 (P13) (Zhang et al., 2004). Episodic dyskinesias have been linked to basal ganglia and cerebellar networks (Neychev et al., 2008) and, along with the ataxic gait, appear after 1 month of age.

To determine whether P/Q-specific deficits arise from channelopathy expressed before or after birth, and to correlate specific channelopathy phenotypes with defined neuronal circuits, we delayed the deletion of the P/Q-type channel in cerebellar PCs by crossing a floxed knock-in line with the postnatally expressed PCP2-Cre line (Barski et al., 2000), resulting in loss of the channel in PCs and sparse loss of the channel in forebrain beginning at 6 d of age. These mice show ataxia, episodic dyskinesia, and absence epilepsy, demonstrating that delayed loss of P/Q-type channels is sufficient to trigger the full disease phenotype.

Materials and Methods

Conditional knock-in

Genomic DNA for construction of the conditional targeting vector was isolated from a RPCI-22 BAC library of 129 DNA in the Genome Resource Facility at the Hospital for Sick Children (Toronto, Ontario, Canada) and verified by extensive Southern blot and sequence analyses. Ten RPCI-22 mouse BAC clones tested positive for the *Cacna1a* region of interest. The NheI restriction sites were used to isolate and directly subclone the 8 and 2 kb fragments into pcDNA3.1(+) (Invitrogen Life Technologies). Positive clones were detected by bacterial lifts with probes to exon 1 (8 kb) or intron 1 (2 kb) and verified by sequence analysis to the mouse genomic sequence reference NM_007578 (University of California, Santa Cruz, CA, Genomic Browser). The conditional targeting vector for *Cacna1a* was designed under the guidance and expertise of Dr. S. O'Gorman (O'Gorman et al., 1997). Briefly, an 8 kb *Cacna1a* genomic DNA was subcloned into pSP72 backbone (Promega). Citrine (Heikal et al., 2000), a third-generation yellow fluorescent protein (YFP) derivative, was flanked on the 5′ end with a loxP and inserted in frame into a SacII site in exon 1. The floxed Citrine insertion is flanked by a 2 kb 5′ untranslated region (short arm) and 6.5 kb intron 1 (long arm) region of homology. To ensure that the position of Citrine in *Cacna1a* does not disrupt the function or distribution of P/Q-type Ca^{2+} channels, a YFP-labeled rat *Cacna1a* cDNA that is over 99% identical to the mouse cDNA in the N-terminal region (100% on protein level) was generated in the same position. Proper physiological function and membrane expression was demonstrated. In addition, a 1.8 kb genomic fragment containing exon 1, Citrine, and part of intron 1 was transiently expressed in HEK293 cells. A fragment of ~65 kDa was produced in HEK293 cells and distributed in a punctate manner to the periphery of the cells. The neomycin gene [pOG277 (O'Gorman et al., 1997)] flanked by loxP sites was inserted into a PvuII site in intron 1 for positive selection of targeted genes, and the HSV thymidine kinase gene [pNT-TK (Tybulewicz et al., 1991)] was inserted into the multiple cloning site of pSP72 backbone (Promega) at HindIII site 5′ to the short arm region of homology as a negative selection for improperly targeted genes. Intronic insertion of a neo gene may decrease levels of *Cacna1a* mRNA and cause premature splicing events. To avoid this problem, the neo cassette was inserted 800 bp downstream from the 5′ end of intron 1 and flanked with loxP sites for subsequent deletion of the gene with Cre recombinase. After linearization of the conditional targeting vector with PvuI, the Transgene and Targeting Service at Case Western Reserve University (Cleveland, OH) targeted the *Cacna1a-Citrine* vector in embryonic stem (ES) cells containing the mouse protamine 1 promotor-Cre recombinase (*PrmCre*) trangenes (O'Gorman et al., 1997). The *Prm1* promoter restricts the expression of Cre to the haploid spermatids in mature mice, therefore reducing the number of electroporations and their time in culture, which increases the chances of ES cells of going germ line. Positively expressing ES cell lines were confirmed by Southern blot analysis. Isolated genomic DNA from potential targeted ES cell lines were digested with BglII and probed with the 5′ and 3′ external probe by Southern blot analyses (see Fig. 1). Successful homologously recombined targeting vectors produced a fragment at 7.5 kb and a WT fragment of 10.8 kb versus unsuccessful neo gene-alone recombinants at 12 kb. Positive ES clones were also confirmed by Southern blot analyses with a 3′ internal probe after BglII digest for proper recombination of the long arm and by PCR and sequence analysis for successful recombination of the loxP sites, Citrine, and neomycin genes. Positive ES cell clones containing the *Cacna1a*-targeted gene were prepared and injected into blastocysts by the standard protocols of the Transgene and Targeting Service at Case Western Reserve University.

ES cells that tested positive for a correct homologous recombination into the *Cacna1a* allele were used for implantation into pseudopregnant mice according to the standard procedures of the Transgenesis and Targeting Service at Case Western Reserve University. Conditional $Cacna1a^{Citrine}$ mice were obtained by a series of matings. Briefly, male chimeras containing the targeted allele and the *PrmCre* transgene were initially mated with several WT females to generate four genetically different offsprings. Only the $Cacna1a^{null(+/-)}$ and $Cacna1a^{Citrine(+/-)}$ females also carrying the *PrmCre* were further mated with WT males to ensure the conservation of the conditional alleles (PrmCre recombinase activity occurs only in the male spermatids) and subsequent replacement of the *PrmCre* with a WT allele. $Cacna1a^{null(+/-)}$ and $Cacna1a^{Citrine(+/-)}$ mice not carrying the *PrmCre* gene were then crossed with each other to obtain complete knock-out mice ($Cacna1a^{null(-/-)}$) or homozygous knock-in mice ($Cacna1a^{Citrine(+/+)}$). $Cacna1a^{Citrine}$ mice were then further crossed with transgenic PC-specific CRE ($Tg^{Pcp2\text{-}cre}$) mice to create the *purky* mice ($Cacna1a^{purky}$). The genetic background of the mice was determined by PCR of genomic DNA from tail biopsy. To detect Citrine incorporation into the *Cacna1* gene, PCRs were performed with primers to *Cacna1a*, *Citrine*, *Cre recombinase*, and *Prm* promoter. The following primer pairs were used to identify the mouse strains described: WT forward 5′ GGGGTCTGACTTCTGATGGA 3′, reverse 5′ AAGTTGCACACAGGGCTTCT 3′; $Cacna1a^{null}$ forward 5′ CCCTTTGCTCTTTGCAGAAT 3′, reverse 5′ CTAAACCCAAGCCCACAAAA 3′; $Cacna1a^{Citrine}$ forward 5′ TATATCATGGCCGACAAGCA 3′, reverse 5′ TTCGGTCTTCACAAGGAACC 3′; $Tg^{Pcp2\text{-}cre}$ forward 5′ ATTCTCCCACCACCGTCAGTACG 3′, reverse 5′ AAAATTTGCCTGCATTACCG 3′; $Tg^{Protamine\text{-}Cre}$ forward 5′ CTGATGCCAAAGCCCTGCCCACCCCTCTCA 3′, reverse 5′ GGACAGAAGCATTTTCCAGGTATGCTCAGA 3′.

Mouse strains

$Tg^{Pcp2\text{-}cre}$ mice [stock number 004146 B6.129-Tg(Pcp2-cre)2Mpin/J (Barski et al., 2000)] and C57BL/6J (stock number 000664) were purchased from The Jackson Laboratory. PrmCre ES cells were a gift from S. O'Gorman, Case Western Reserve University, Cleveland, OH (O'Gorman et al., 1997).

Immunohistochemistry, antibodies, and analysis

Animals were anesthetized and perfused intracardially with 4% paraformaldehyde in PBS. Three female mouse brains per genotype at 3 months of age were removed and fixed for 1 h at 4°C and cryoprotected overnight by incubating in 30% (w/v) sucrose in PBS. Samples were embedded in OCT and immediately frozen in dry ice. Twenty-micrometer cryostat sections were collected and air dried at room temperature on gelatin-coated slides. Immunofluorescent labeling was performed according to standard procedures established in our laboratory (Mark et al., 1995). The following primary and secondary antibodies were used: anti-calbindin-D (Swannt), anti-P/Q-type Ca^{2+} channel (Synaptic Systems), anti-green fluorescent protein (GFP) (Millipore and Invitrogen), α-bungarotoxin conjugated to Alexa 594 (Invitrogen), anti-rabbit Alexa 647 (Invitrogen), and anti-chicken FITC (Jackson ImmunoResearch). Antibodies were used to label the various tissues. Sagittal slices were incubated with the primary antibody overnight at 4°C, washed, and incubated with the secondary antibody (Invitrogen) for 2 h at room temperature to overnight at 4°C. Cells were embedded in Prolong Gold antifade (Invitrogen). Images were acquired with a Zeiss LSM 510 confocal microscope and analyzed using VOLOCITY software (Improvision). For quantification of P/Q-type channel staining in cerebellar slices (see Fig. 4), images were acquired using the same settings on the LSM 510. Regions of interest (soma or dendrites) were selected, the average pixel intensity was measured, and the ratio between the red channel and the green channel was determined.

For P/Q-type channel staining in thalamocortical slices (see Fig. 8*C*), brains were sliced coronally from three (two females and one male) mice per genotype at 6–9 months of age and incubated overnight at 4°C with primary antibodies (anti-parvalbumin, 1:1000, Millipore; and anti-P/Q type channel, 1:500, Synaptic Systems) and secondary antibodies (donkey anti mouse 549 and donkey anti rabbit 488; both Jackson ImmunoResearch Laboratories). Pictures were taken on a BX51 microscope (Olympus) equipped with a SPOT RT camera (Diagnostic Instruments).

Western blots from adult *Cacna1a*^{Citrine} and *Cacna1a*$^{purk(-/-)}$ mouse brain homogenates were performed according to the methods of Han et al. (2006). The cerebellum from three female mice per genotype or the forebrain from three female and two male mice per genotype from age 6–9 months were used. Anti-$Ca_V2.1$ (1:200) was purchased from Millipore, and anti-actin (1:500) was purchased from Sigma-Aldrich. Relative protein expression was analyzed with VOLOCITY software (Improvision) from three independent blots.

Relative sizes of cerebellar structures from wild-type (WT) *Cacna1a*^{Citrine} and *Cacna1a*$^{purk(-/-)}$ sagittal cerebellar sections were analyzed using VOLOCITY software (Improvision). At least three 3-month-old female mice per genotype were used. The area of sagittal cerebellar sections and the thickness of the molecular and granular layers were measured, and the mean values from *Cacna1a*^{Citrine} and *Cacna1a*$^{purk(-/-)}$ were compared to WT values. Statistical significance was evaluated with *the t* test. Standard errors are mean ± SEM.

Videoelectroencephalographic recordings

Silver wire electrodes (0.005 inch diameter) attached to a microminiature connector were implanted bilaterally into the subdural space over the frontal, temporal, parietal, and occipital cortices of mice under Avertin anesthesia. After surgery, mice were allowed to recover for at least 1 d before recording. Simultaneous cortical EEG activity and behavioral video monitoring were performed using a digital electroencephalograph (Stellate Systems). EEGs were recorded for more than 2 h/d over multiple days. Recordings were made from four or more male mice per genotype. Mice were evaluated between the ages of 1 and 4 months. EEG signals were filtered through a 3 Hz high-pass filter, a 35 Hz low-pass filter, and a 60 Hz notch filter.

Ca^{2+} channel recordings in HEK293 cells. The P/Q-type Ca^{2+} channel subunits ($Ca_v\alpha_1 2.1$, $Ca_v\beta_{1b}$, and $Ca_v\alpha_2\delta$) were a kind gift from Dr. T. Snutch (University of British Columbia, Vancouver, British Columbia, Canada). The YFP tag was inserted into the SacII site of the rat $Ca_v\alpha_1 2.1$ subunit. The tagged and untagged form of $Ca_v\alpha_1 2.1$ were coexpressed with $Ca_v\beta_{1b,}$ and $Ca_v\alpha_2\delta$ subunits in HEK293 cells. Cells were transfected at a molar ratio of 1:1:1. Transfection was performed according to manufacture procedures using Cytofectene reagent (Bio-Rad). Whole-cell patch-clamp recordings were performed on an EPC9–2 patch-clamp amplifier. Currents were digitized at 10 kHz and filtered with the internal 10 kHz three-pole Bessel filter in series with a 2.9 kHz four-pole Bessel filter of the EPC9 amplifier. Series resistances were partially compensated between 70 and 90%. Leak and capacitative currents were subtracted using hyperpolarizing pulses from −60 to −70 mV. Experiments were performed using extracellular (in mM: 100 Tris, 4 $MgCl_2$, and 10 $BaCl_2$) and intracellular (in mM: 120 aspartic acid, 5 $CaCl_2$, 2 $MgCl_2$, 10 HEPES, 10 EGTA, and 2 Mg-ATP; buffered with CsOH to pH 7.3) solutions.

Ca^{2+} channel current recording in dissociated PCs. Dissociated PCs were prepared with an enzymatic isolation technique from mutant mice (four WT, seven *Cacna1a*^{Citrine}; four *Cacna1a*$^{Null(-/-)}$, eight *Cacna1a*$^{purk(-/-)}$; gender not determined) aged 13–28 d postnatally (Mintz et al., 1992b; Raman and Bean, 1997, 1999). Current recordings were further analyzed and divided by age in Figure 4*D*. For this study, three *Cacna1a*^{Citrine} mice at P14, four *Cacna1a*^{Citrine} mice at P23–P28, three *Cacna1a*$^{purk(-/-)}$ mice at P14–P15, and five *Cacna1a*$^{purk(-/-)}$ mice at P17–P22 were used (gender not determined). Mice were deeply anesthetized with isoflurane and decapitated. The cerebellar vermis was removed, cooled, and sliced parasagittally in 400-μm-thick sections with a Vibratome (VT1000S; Leica) in ice-cold artificial CSF (ACSF) containing (in mM) 125 NaCl, 2.5 KCl, 2 $CaCl_2$, 1 $MgSO_4$, 1.25 NaH_2PO_4, 26 $NaHCO_3$, and 20 glucose bubbled with 95% O_2 and 5% CO_2. The slices were incubated in warm dissociation solution (82 mM Na_2SO_4, 30 mM K_2SO_4, 5 mM $MgCl_2$, 10 mM HEPES, 10 mM glucose, and 2.5 mg/ml protease XXIII, pH 7.4, adjusted with NaOH) at 35°C for 5 min and washed in the ice-cold dissociation solution containing 1 mg/ml bovine serum albumin and 1 mg/ml trypsin inhibitor. To isolate PCs, the slices were minced by gentle trituration with a fire-polished Pasteur pipette in Tyrode's solution containing (in mM) 150 NaCl, 4 KCl, 2 $CaCl_2$, 2 $MgCl_2$, 10 HEPES, and 10 glucose (pH 7.4, adjusted with NaOH). PCs were identified by their large diameter and characteristic pear-like shape caused by the severed dendritic tree. Whole-cell recordings were made with an EPC9/2 amplifier (HEKA) at room temperature from the cells that were tightly settled on culture dishes and exposed externally to a stream of focally applied solution consisting of 160 mM tetraethylammonium chloride (TEA-Cl), 2 mM $BaCl_2$, 10 mM HEPES, 10 mM glucose, 1 mM TTX, and 0.1 mg/ml cytochrome *c* (pH 7.4 adjusted CsCl). Patch pipettes (1–3 MΩ) were filled with an internal solution with the following composition (in mM: 90 $CsMeSO_3$, 10 HEPES, 10 EGTA, 0.5 $CaCl_2$, 4 $MgCl_2$, 4 Na-ATP, 0.4 Na-GTP, 2 QX314, 20 TEA-Cl, and 10 Tris-phosphocreatine, pH 7.3, adjusted with CsOH). The Pulse software (HEKA) was used to control membrane voltage and data acquisition. The cells were voltage clamped at −70 mV and depolarized every 10 s to −10 mV for 30 ms to activate VGCCs. Membrane currents were filtered at 3 kHz and digitized at 20 kHz. Series resistance was routinely compensated by 70–80%. Off-line analysis was performed with Igor Pro software (Wavemetrics). Current traces were corrected by subtracting the leakage and the capacitive current with the P/6 method. ωAgatoxin IVA, ωConotoxin GVIA (Peptide Institute), and nimodipine (Sigma) were freshly dissolved in external solution just before application.

Extracellular recordings of spontaneous activity in PCs. To examine the firing properties of PCs, we used extracellular recording methods as described previously (Edwards et al., 1989; Womack and Khodakhah, 2003). Briefly, brains from three male mice per genotype were removed after decapitation and incubated immediately in ice-cold ACSF. The cerebellum was dissected, and sagittal slices (300 μm) were cut on a VT1000S vibratome (Leica). Slices were incubated for 30 min at room temperature before recording and perfused with ACSF (pH 7.35; in mM: 128 NaCl, 3 KCl, 2.5 $CaCl_2$, 1.2 $MgSO_4$, 26 $NaHCO_3$, 1.23 NaH_2PO_4 and 10 D-glucose) equilibrated with 95% O_2 and 5% CO_2. To block excitatory and inhibitory synaptic input onto PCs, slices were perfused continuously with 6-cyano-7-nitroquinoxaline-2,3-dione disodium (CNQX; 10 μM; Tocris) and picrotoxin (100 μM; Tocris). PC neurons were identified by their characteristic morphology using infrared optics. Experiments were performed at 35 ± 0.5°C using a heated slice chamber in combination with a temperature controller (WPI). Extracellular recordings were analyzed with IgorPro. Spike detection, calculations of interspike intervals, and generation of interspike interval histograms were performed using a customized analysis protocol. The raw trace of each recording was first digitally filtered in Igor using a low-pass 1 kHz filter (FilterFIR; IgorPro) with the following parameters: the end of the pass band frequency was set to 0.02; the start of the reject band was set to 0.021; and the number of FilterFIR coefficients was set to 101. Spikes were then detected in the extracellular trace using an automated scanning protocol to detect a downward deflecting peak in each 5 s trace in 5 ms window steps. Downward deflecting peaks whose value exceeded the average value of the trace in each window by >200 μV were defined as spikes. The interspike interval was then calculated by subtracting the difference between arrival times of the $(i + 1)$th and ith spikes. Histograms (128 bins) of the interspike intervals were then generated using the histogram analysis function within Igor. Bin width was set to 0.5 ms. Interspike intervals for cells with the trimodal pattern of activity were only analyzed during the tonic epoch of activity.

IPSC recordings of cerebellar and thalamic nuclei. Recording were made of IPSCs in deep cerebellar nuclei and lateral dorsal thalamic nucleus. Parasaggital slices (300 μm thick) of cerebellum (five *Cacna1a*^{Citrine} and six *Cacna1a*$^{purk(-/-)}$; gender not determined) and thalamus (seven *Cacna1a*^{Citrine} and four *Cacna1a*$^{purk(-/-)}$; gender not determined) were prepared from mutant mice aged 14–18 d postnatally and 18–25 d postnatally, respectively. Neurons in the deep cerebellar nucleus (DCN) and LD thalamic nucleus were visually identified under an upright microscope (DMLFSA; Leica) equipped with infrared illumination. Whole-cell

recordings were made at room temperature under continuous perfusion of ACSF including 10 μM CNQX (Tocris), 20 μM D-(−)-2-amino-5-phosphonopentanoic acid (Tocris), and 0.5 μM strychnine (Tocris). Patch pipettes (1–3 MΩ) were filled with an internal solution with the following composition (in mM): 135 CsCl, 10 HEPES, 1 EGTA, 0.1 $CaCl_2$, 4 $MgCl_2$, 4 Na-ATP, 0.4 Na-GTP, 2 QX314, and 10 Tris-phosphocreatine (pH 7.3, adjusted with CsOH). The cells were voltage clamped at −70 mV with an EPC10/2 amplifier (HEKA). Membrane currents were filtered at 3 kHz and digitized at 20 kHz. The PatchMaster software (HEKA) was used to control membrane voltage stimulation, timing, and data acquisition. Series resistance was routinely compensated by 70–80%. Synaptic transmission was evoked by 100 μs voltage pulses applied through a glass pipette filled with ASCF. The stimulation pipette was positioned in the vicinity of the corticonuclear tract containing a dense PC axon bundle and in the vicinity of the reticular nucleus thalami. ωAgatoxin IVA and ωConotoxin GVIA were dissolved in ACSF containing cytochrome *c* (1 mg/ml) just before bath application.

Statistical significance in all experiments was evaluated with ANOVA using Igor Pro (Wavemetrics) software. Standard errors are mean ± SEM.

In vivo *recordings.* Extracellular recordings were performed to elucidate differences in PC activity between WT ($n = 6$; four males and two females), *Cacna1a*^{Citrine} ($n = 3$; one male and two females), and *Cacna1a*$^{purk(-/-)}$ ($n = 3$; three males) mice. Males and females 6–12 months of age were used. For the *in vivo* recordings, the mice were anesthetized (isoflurane, 1.5–3%; CP Pharma), and analgesia was supported by Fentanyl (0.08 mg/kg body weight; Curasan) and placed in a stereotactic frame (Narishige). A sagittal incision along the midline was made to expose the cranium, and a burr hole was drilled 6 mm posterior to the bregma to allow access to the vermis. Spontaneous activity of PCs was recorded with a multielectrode system (Thomas Recording), and extracellular signals of up to four electrodes (impedance, 1–2 MΩ at 1 kHz; Thomas Recording) were simultaneously amplified and filtered (bandpass, 0.5–9 kHz) with a multichannel spike sorter (Plexon). All signals were sampled with high temporal resolution (32 kHz). In the off-line analysis, simple spikes and complex spikes were detected and discriminated using custom-made software implemented in Matlab (MathWorks). Time series of single-cell spikes were used for further processing to calculate mean firing rates, interspike interval distributions, and SD of interspike intervals. To quantify the variability in spike activity, we calculated the coefficient of variation (CV) of interspike intervals (CV = SD of interspike intervals /mean of interspike intervals). Statistical significance in the experiments was evaluated with the Mann–Whitney *U* test. Standard errors are mean ± SEM.

Behavioral analysis

Gait analysis. The CatWalk 7.1 system (Noldus Information Technology) was used to assess ataxia and gait abnormalities from the footprints of three male mice per genotype at 3 months of age in locomotion. Mice were placed on one end of the catwalk and encouraged to walk down the walkway at a constant speed without interruptions. Each individual paw contact on the walkway was recorded by video camera. Images were then automatically analyzed by the CatWalk software and with ink print analysis. Stride length was measured and reported as mean ± SEM.

Basso Mouse Scale for locomotion. To assess the locomotor abilities of mice lacking the P/Q-type channel in PCs, six male mice per genotype at 6 months of age were tested using a modified version of the open-field Basso Mouse Scale (BMS) and subscore (Basso et al., 2006). Averages from the BMS scores, subscores, and a combination of both scores were calculated.

Rotarod. Motor coordination and balance skills were assessed by a rotarod test (Columbus Instruments). At least four 3-month-old male mice per genotype were placed on a rod rotating at 4 rpm for 1 min acclimation. The rod was then accelerated at 0.1 rpm/s up to 40.0 rpm. The test continued until all mice had fallen off the rod. Latency to fall and revolutions per minute at the time of the fall were recorded for each mouse. Three trials per mouse were run and averaged together.

Vertical pole test. Motor coordination and balance skills were assessed also by the vertical pole test. A 50 cm grooved plastic pole (diameter, 1 cm) was placed vertically and secured to a platform. The animal was placed faced upward, at the top of the pole, and the latency to turn around and climb down the vertical pole was recorded. Time out occurred if the mouse did not complete the task after 120 s. If the mouse fell from the top of the pole, a time of 120 s and a "fall" notation was recorded. At least five 6-month-old male mice per genotype were used.

Incline screen test. Coordination, muscle strength, and balance were tested with the incline screen test. Two wire mesh screens, one at a 60° angle and the other at a 90° angle were used for this test. The mouse was placed facing downward in the middle of the screen. Latency to turn around and climb to the top was recorded. Maximum latency to complete the task was set at 60 s. If the mouse fell, a time of 60 s and a fall notation were recorded. Six 6-month-old male mice per genotype were used.

Grip strength test. Muscle strength of forelimbs and combined forelimb–hindlimb grip strength of mice were measured using a commercially available grip strength meter apparatus (San Diego Instruments). The system is supplied with a double grid (400 × 180 × 200 mm) that connects to the sensor. Briefly, the mouse was removed from its home cage by gripping the base of the tail between thumb and forefinger. The mouse was gently lowered over the top of the grid so that only its front paws could grip the wire grid. Keeping the torso horizontal, the mouse was pulled until the grip was released, and the value of the maximal grip strength displayed on the screen (grams of force) was noted. The test was repeated five times for both forepaws and hindpaws at 5 min intervals between animals, and the peak grip strength measurement was selected for statistical analyses. At least six 6-month-old male mice per genotype were used.

Statistical significance throughout all behavior experiments was evaluated with the ANOVA test. Standard errors are mean ± SEM.

Characterization of dystonic episodes. Adult male and female *Cacna1a*^{Citrine} and *Cacna1a*$^{purk(-/-)}$ mice between 3 and 18 months of age were monitored in a test cage. The number of mice used for each test is indicated in Table 2. After 2 h of acclimation, spontaneous dystonic episodes (4 females and 4 males, *Cacna1a*^{Citrine}; 10 females and 8 males, *Cacna1a*$^{purk(-/-)}$) were video recorded with Ethovision software by Noldus, and the frequency and duration of attacks over a 24 h period were recorded and reported as an average daily rate. Stress- or chemical-induced dystonic episodes were monitored in mice every 5–10 min for 60 min (or until the episode ended) after a change from their home cage (18 females and 9 males, *Cacna1a*^{Citrine}; 4 females and 10 males, *Cacna1a*$^{purk(-/-)}$), a 10 min cage transport on a laboratory cart (18 females and 9 males, *Cacna1a*^{Citrine}; 4 females and 10 males, *Cacna1a*$^{purk(-/-)}$), a short 10 min restraint in a 100 ml syringe (18 females and 9 males, *Cacna1a*^{Citrine}; 4 females and 10 males, *Cacna1a*$^{purk(-/-)}$), a subcutaneous injection of 0.9% NaCl as a vehicle control (13 females and 9 males, *Cacna1a*^{Citrine}; 4 females and 10 males, *Cacna1a*$^{purk(-/-)}$), a subcutaneous injection of 15 mg/kg caffeine (3 females and 8 males, *Cacna1a*^{Citrine}; 3 females and 10 males, *Cacna1a*$^{purk(-/-)}$), and an intraperitoneal injection of 2 g/kg ethanol (3 females and 8 males, *Cacna1a*^{Citrine}; 3 females and 10 males, *Cacna1a*$^{purk(-/-)}$). Behavioral studies were performed according to the methods of Fureman et al. (2002). Data represent the percentage of mice that had a dystonic episode per mouse group and the average episode duration per group. Statistical significance was evaluated with the ANOVA test.

Throughout the experiments, $^{*}p < 0.05$ and $^{**}p < 0.01$.

Results

Creating a conditional Citrine-tagged P/Q-type channel knock-in for the visualization and cell-type-specific knockdown of Cacna1A

To study the distribution and function of P/Q-type channels in living mice, we engineered a conditional knock-in mouse model in which the P/Q-type channel can be visualized and deleted from a specific cell type. As indicated in Figure 1*A*, we inserted a GFP variant, Citrine (Heikal et al., 2000), in frame within the first exon of the *Cacna1a* gene. This insert adds a Citrine tag to the Cacna1A subunit protein with a 12 amino acid linker on its amino terminal end representing the translation of an engineered loxP site. Two additional loxP sites flanking the neomycin gene are located

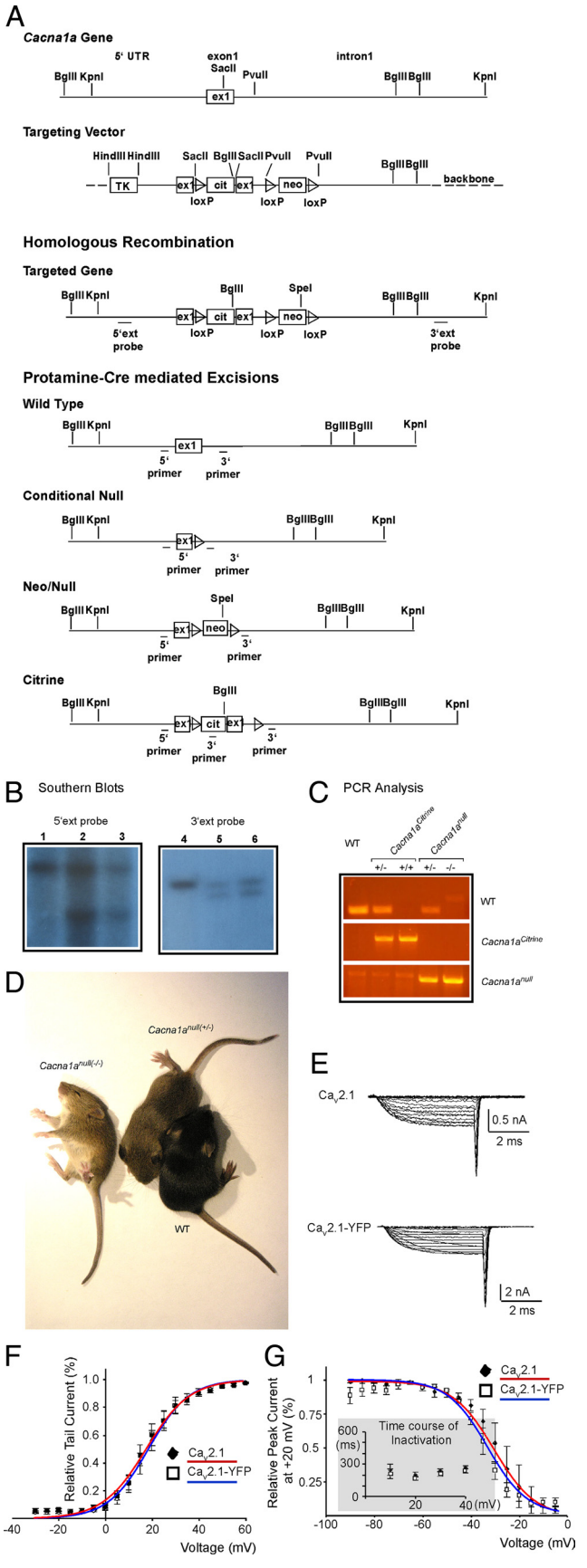

Figure 1. Creating *Cacna1a*^{Citrine} mice. ***A***, Design of the targeting vector to create *Cacna1a*^{Citrine} mice. The WT gene with exon 1 (ex1) flanked by the 5′ untranslated region (UTR), and intron 1 is depicted at the top, the targeting vector in the second line and the correctly targeted gene in the third line. An 8 kb *Cacna1a* fragment was subcloned into pSP72 backbone (Promega). *Citrine* gene (cit) flanked by a loxP site on the 5′ end was subcloned into a SacII site in exon 1. *Neomycin* (neo) gene was subcloned into a PvuII site 800 bp downstream from the Citrine insertion in intron 1. *Thymidine kinase* (TK) gene was subcloned in a HindIII site in the pSP72 backbone. Male chimeras containing the targeted allele and the PrmCre transgene were mated with several WT females to generate four genetically different offspring: wild type, conditional null, Neo/null, and Citrine. Detection strategy of the conditional knock-in and knock-out mice by PCR after Cre recombinase excision by Protamine-CRE is shown in the schematic. ***B***, Southern blot analyses for the detection of correctly targeted genes. Isolated genomic DNA from potentially targeted ES cell lines was digested with BglII and probed with the 5′ external (lanes 1–3) or digested with KpnI and SpeI and probed with a 3′ external (lanes 4–6) probe. Lanes 1 and 4 are bands expected from WT ES cells, lanes 2 and 5 are bands expected from a positive clone G3, and lanes 3 and 6 are bands expected from a positive clone H5. Successful homologously recombined targeting vectors produced a fragment at 7.5 kb (lanes 2 and 3, top blot) and a WT fragment of 10.8 kb (lanes 1–3, top blot) with the 5′ external probe and a 11.4 kb (lanes 5 and 6, bottom blot) and a WT fragment of 14.4 kb (lanes 4–6, bottom blot) with the 3′ external probe. ***C***, PCR analysis and distinction between WT, *Cacna1a*^{Citrine}, and *Cacna1a*$^{null(-/-)}$ mice. Depiction of PCR results from a WT, *Cacna1a*^{Citrine}, and *Cacna1a*$^{null(-/-)}$ mice with three different primer combinations, specific for detecting the different mouse genotypes. ***D***, Phenotypic differences between WT, *Cacna1a*^{Citrine}, and *Cacna1a*$^{null(-/-)}$. Whereas WT and *Cacna1a*^{Citrine} reveal similar phenotypes, the *Cacna1a*$^{null(-/-)}$ mice develop severe seizures and die within 3–4 weeks after birth. ***E–G***, N-terminally YFP-tagged $Ca_v2.1$ channels reveal the same biophysical properties as the untagged channels. The YFP tag was inserted into the conserved SacII site, which is the corresponding position in exon 1 of the mouse gene. HEK293 cells were cotransfected with either $Ca_v\alpha_1 2.1$ (untagged) or $Ca_v\alpha_1 2.1$-YFP plus $Ca_v\beta_{1b}$ and $Ca_v\alpha_2\delta$ subunits, and whole-cell patch-clamp recordings were performed 12–24 h after transfection. ***E***, Examples of current traces of untagged (top) or YFP-tagged (bottom) $Ca_v2.1$ channels used for voltage dependence of activation analysis as shown in ***F***. ***F***, Voltage dependence of activation of $Ca_v2.1$ channels. ***G***, Voltage dependence of inactivation of $Ca_v2.1$ channels. Inset, Inactivation time constants determined by indicated voltage pulses for a 1 s test pulse. There were no differences in peak current amplitude between the tagged and untagged channels (Cav2.1 untagged: 684 ± 216 pA, $n = 36$; Cav2.1-YFP (SacII): 710 ± 356 pA, $n = 13$).

within the first 1 kb of intron 1. The Citrine allows the visualization of the P/Q-type channel α_1 subunit, whereas the loxP sites can be used to delete the expression of the P/Q-type channel protein using Cre recombinases. Before constructing the targeting vector, we verified that the insertion of the Citrine GFP variant at the corresponding N-terminal site in the rat and human recombinant P/Q-type channel does not interfere with the biophysical properties of the channel in HEK293 cells (Fig. 1*E–G*) (see also Hummer et al., 2003). Neither the activation nor the inactivation properties were altered by the variant. Having established that the fluorescent protein does not interfere with P/Q-type current, we created the *Cacna1a*$^{tm\text{-}Citrine+/+}$ mice using homologous recombination (see Materials and Methods). Briefly, the *Cacna1a-Citrine* vector was targeted in ES cells containing the mouse protamine 1 promotor-Cre recombinase (*PrmCre*) (O'Gorman et al., 1997) transgene. The PrmCre recombinase activity is restricted to haploid spermatids, which results in functional deletion of the P/Q-type channel in the first generation (Fig. 1*A*). Deletion of the complete P/Q-type channel by the Prm1-Cre recombinase resulted in a null phenotype as described previously (Jun et al., 1999; Fletcher et al., 2001; Todorov et al., 2006). These mice are smaller than WT mice, are ataxic, and develop severe seizures and die 3–4 weeks after birth (from now on called *Cacna1a*$^{null(-/-)}$) (Fig. 1*D*; supplemental Movie 1 (available at www.jneurosci.org as supplemental material). Functional deletion of the neomycin gene by *PrmCre* results in mice bearing a floxed Citrine P/Q-type channel knock-in (*Cacna1a*$^{tm\text{-}Citrine+/+}$; from now on called *Cacna1a*^{Citrine}). These mice are viable, fertile, and indistinguishable from their WT littermates (supplemental Movie 2, available at www.jneurosci.org as supplemental material). To verify the correct distribution of the Citrine-tagged P/Q-type channel, we used

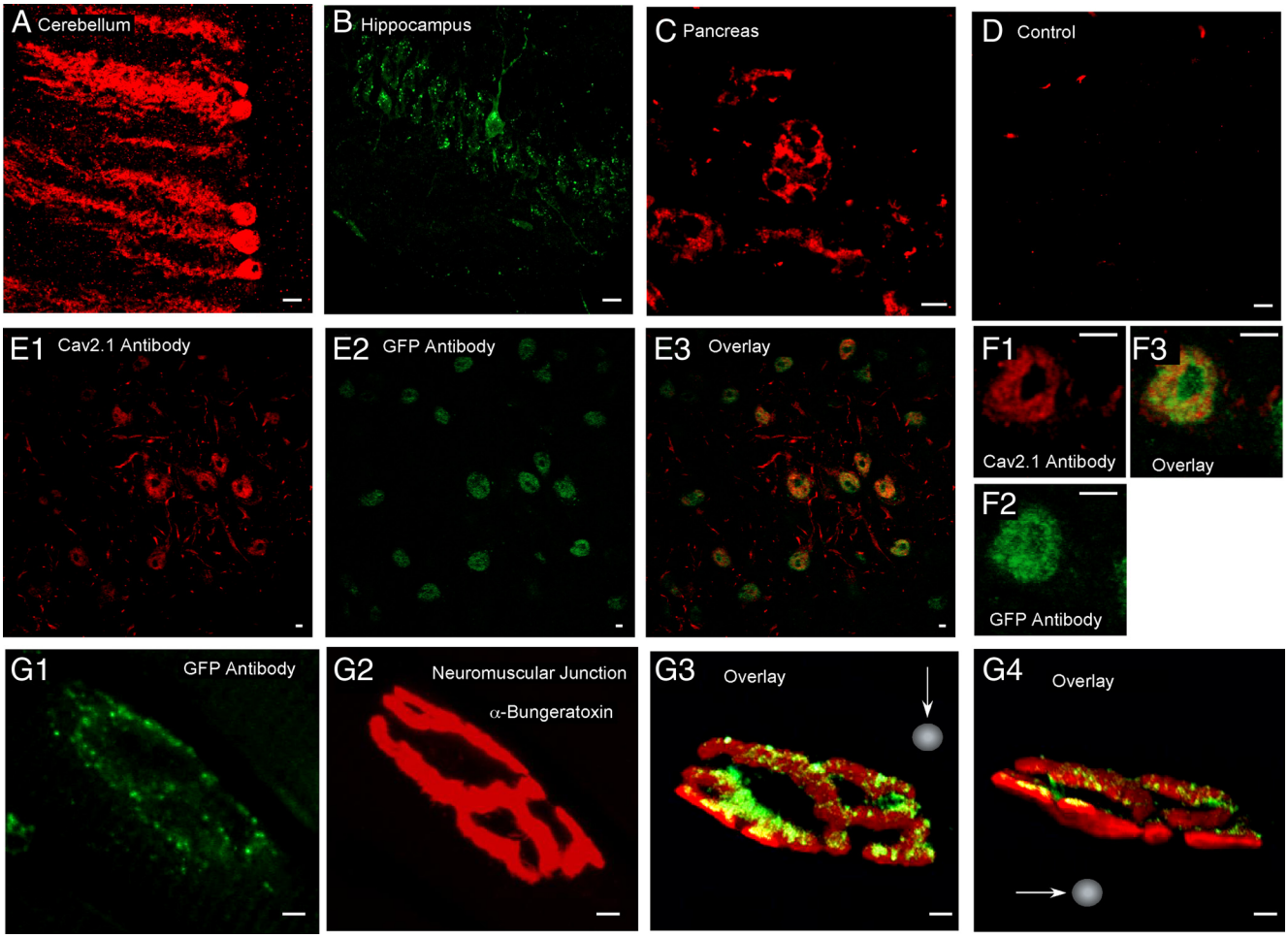

Figure 2. Visualization of P/Q-type channel protein using the Citrine tag of *Cacna1a*^{Citrine} mice. ***A–D***, Distribution of P/Q-type channels tagged with Citrine in the brain and pancreas. Shown are images of cerebellar PCs (***A***) from founder mice, hippocampal CA1 region (***B***) from founder mice, pancreas (islet cells; ***C***) from founder mice, and cerebellar PCs (***D***) from C57/B6 control mice. Sagittal frozen sections from adult female brains and pancreas were taken from founders (***A–C***) or C57/B6 mice as control (***D***). Brain and pancreas sections were incubated with rabbit anti-GFP antibody (Invitrogen) and goat anti-rabbit Alexa 647 secondary antibody (***A***, ***C***, ***D***) or with chicken anti-GFP (Millipore) and donkey anti-chicken FITC (***B***) to identify P/Q-type Ca^{2+} channels. ***E***, ***F***, Colocalization of Cacna1a^{Citrine} channels in the hippocampus detected with Cacna1A antibodies (***E1***, ***F1***) and GFP antibodies (***E2***, ***F2***). The overlay in ***E3*** and ***F3*** reveals that both antibodies detect the same protein. ***G***, Distribution of P/Q-type channels tagged with Citrine at the neuromuscular junction (NMJ). Confocal images of an NMJ costained with α-bungarotoxin (***G2***) and the GFP antibody (***G1***). ***G3–G4***, Three-dimensional reconstruction of confocal *z*-stack images of the NMJ in ***G1*** and ***G2*** illustrate that Citrine-tagged P/Q-type channels are accurately localized presynaptically within the motoneuron, whereas nicotinic acetylcholine receptor are localized postsynaptically at the NMJ. Longitudinal frozen sections from adult muscle were taken from founders and incubated with chicken anti-GFP (Millipore) and donkey anti-chicken FITC (Jackson ImmunoResearch Laboratories) to identify P/Q-type Ca^{2+} channels. Neuromuscular junctions were labeled with α-bungarotoxin conjugated to Alexa 594 (Invitrogen) to identify endplates. Scale bars, 10 μm.

a GFP antibody to analyze various tissue and brain regions from *Cacna1a* $^{tm\text{-}Citrine+/-}$ female founder mice at 3 months of age where P/Q-type channels are typically expressed (i.e., cerebellum, hippocampus, pancreas, and neuromuscular junction) (Herlitze et al., 2003). As shown in Figure 2, the Citrine tag can be detected with the GFP antibody in all tissues analyzed and colocalizes with the endogenous P/Q-type channel. Thus, our results demonstrate that insertion of the floxed Citrine construct into the first exon of the $Ca_v2.1$ channel does not grossly interfere with the developmental function of the channel *in vivo*, allows for the visualization of native P/Q-type channels in brain sections using GFP antibodies, and permits conditional deletion of P/Q-type channels using the promotor-specific expression of Cre-recombinases.

PC selective knockdown of P/Q-type channels in mouse cerebellum

We next used the Tg$^{PCP2\text{-}cre}$ mouse line to ablate P/Q-type channels in cerebellar PCs (Barski et al., 2000). The *PCP2/L7* promotor has been widely used for the PC-specific expression or knockdown of proteins (Oberdick et al., 1990; Burright et al., 1995; Feil et al., 2003; Levin et al., 2006; Wulff et al., 2009). In mice, the *PCP2/L7* promotor is activated around P6 and fully established by 2–3 weeks after birth, with expression in PCs as well as a low level of sparsely scattered, as yet poorly defined forebrain cells (Oberdick et al., 1990; Barski et al., 2000). After crossing the Tg$^{PCP2\text{-}cre}$ mouse line with *Cacna1a*$^{tm\text{-}Citrine+/+}$ mice, we analyzed the behavioral phenotypes and correlated them with the distribution and physiological function of the PCs and the cerebellum over a 6 month time period. Because of their lively attitude despite their postnatal-onset P/Q-type channelopathy, we call these mice *purky* (*Cacna1a*$^{purk(-/-)}$).

Phenotypic analysis

Gross neuroanatomy

We first investigated the gross anatomy of the WT, *Cacna1a*^{Citrine}, and *Cacna1a*$^{purk(-/-)}$ mouse brains at 3 months old. As shown in Figure 3*C*, isolated forebrains are comparable in general structure, size, and weight; however, analysis of cerebellar structures

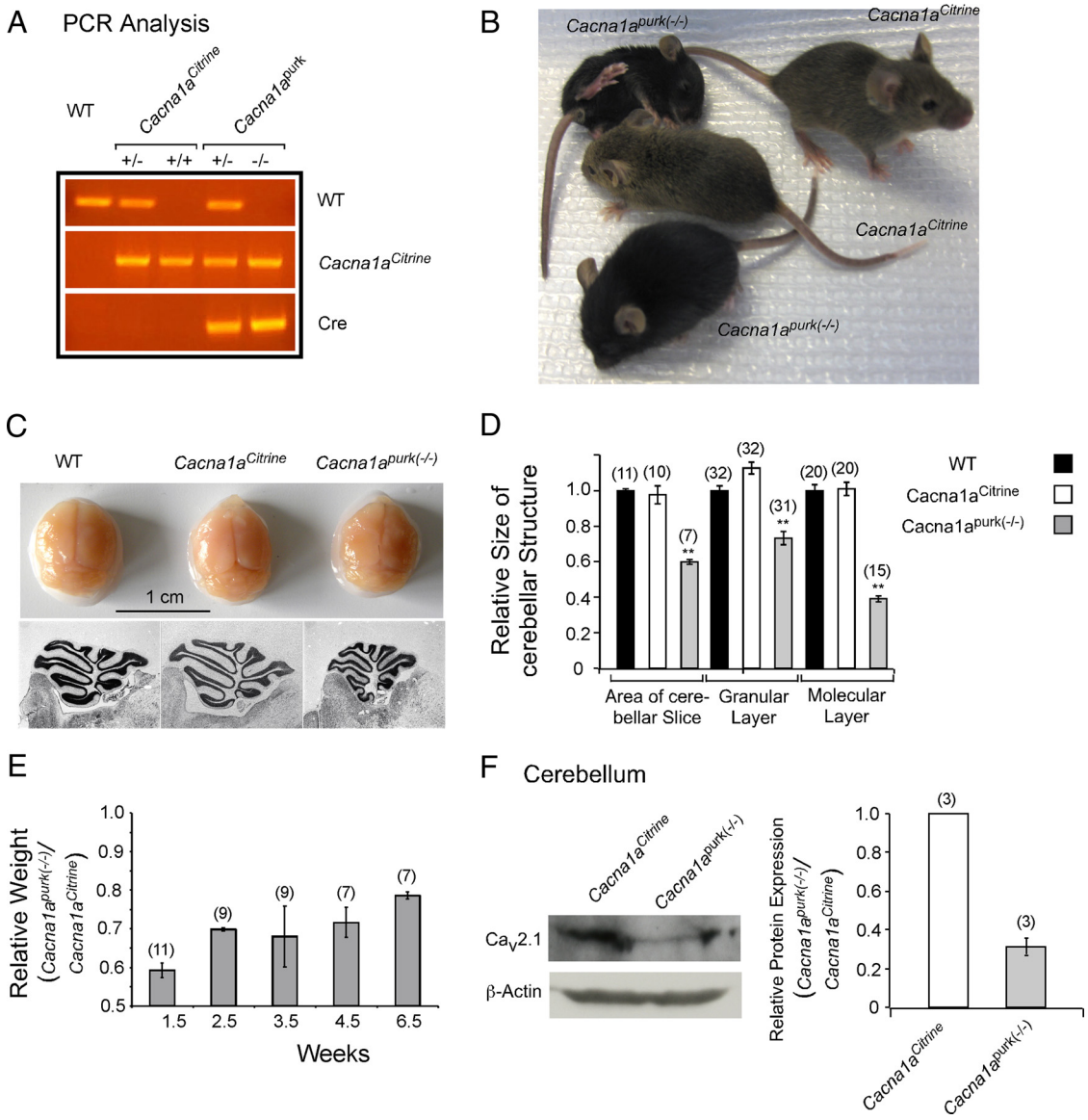

Figure 3. Conditional knockdown of P/Q-type channels in mouse brain. ***A***, PCR analysis and distinction between WT, *Cacna1a*^{Citrine}, and *Cacna1a*$^{purk(-/-)}$ mice. Depiction of PCR results from a WT, *Cacna1a*^{Citrine}, and *Cacna1a*$^{purk(-/-)}$ mice with three different primer combinations, specific for detecting the different mouse genotypes. ***B***, Phenotypic differences between *Cacna1a*^{Citrine} and *Cacna1a*$^{purk(-/-)}$ mice. *Cacna1a*$^{purk(-/-)}$ mice are smaller and develop dystonic episodes after 3 postnatal weeks. ***C***, Comparison of brains and the cerebellar histology of WT, *Cacna1a*^{Citrine}, and *Cacna1a*$^{purk(-/-)}$ mice at 6 months of age do not show differences in gross anatomy, but the cerebellum of *Cacna1a*$^{purk(-/-)}$ is smaller in size. Sagittal sections of the cerebellar vermis were stained with neutral red. ***D***, Relative size of cerebellar structures (area of cerebellar slices, granular layers, and molecular layers) determined in *Cacna1a*^{Citrine} and *Cacna1a*$^{purk(-/-)}$ compared with WT cerebellar slices. ***E***, Comparison of the body weight reveals that *Cacna1a*$^{purk(-/-)}$ mice weigh 40% less than *Cacna1a*^{Citrine} mice 1.5 weeks after birth and 20% less after 6.5 weeks. ***F***, Right, Western blot analysis of cerebellar homogenates from adult *Cacna1a*^{Citrine} and *Cacna1a*$^{purk(-/-)}$ mouse brains (right). Left, Relative protein expression of Cacna1A and β-actin used as a loading control was determined. The number in parentheses indicates the number of experiments.

revealed that the size of the cerebellum as well as its granular and molecular layers are 40–60% smaller in *Cacna1a*$^{purk(-/-)}$ compared with *Cacna1a*^{Citrine} and WT littermates (Fig. 3*D*). In addition, *Cacna1a*$^{purk(-/-)}$ mice weigh significantly less than their *Cacna1a*^{Citrine} littermates, with bodyweights 60% that of their WT, *Cacna1a*^{Citrine}, and *Cacna1a*$^{purk(+/-)}$ littermates after 1.5 weeks and 80% that of their littermates at 6.5 weeks postnatal (Fig. 3*E*), suggesting an early impairment in nourishment caused by cerebellar dysfunction.

PC physiology

To evaluate the effects of delayed Cacna1A ablation on PC signaling and cerebellar cortical outflow in *Cacna1a*$^{purk(-/-)}$ mice, we analyzed somatic P/Q-type channel currents, PC excitability, concentrating on spontaneous impulse activity, and synaptic transmitter release.

Reduction of P/Q-type channel current in PCs. To confirm the loss of P/Q-type Ca^{2+} channels in cerebellar PCs, we analyzed somatic P/Q-type channel current density in acutely dissociated PCs from WT, *Cacna1a*^{Citrine}, *Cacna1a*$^{purk(-/-)}$, and *Cacna1a*^{null} mice (Fig. 4*A–D*). We used enzymatically isolated PCs, which primarily eliminates the dendritic arbors and allows for high-quality voltage-clamp and pharmacological manipulations. We found that the total VGCC current at the soma was greatly reduced in *Cacna1a*$^{purk(-/-)}$ and *Cacna1a*^{null} mice compared with WT and *Cacna1a*^{Citrine} mice (Fig. 4*C*). In WT and *Cacna1a*^{Citrine} mice, the total current consisted almost completely of high-threshold P/Q-type channel current since ωAgaIVA, a selective P/Q-type channel blocker, inhibited over 90% of the total Ca^{2+} current (WT: 94 ± 2%, $n = 4$; *Cacna1a*^{Citrine}: 91 ±

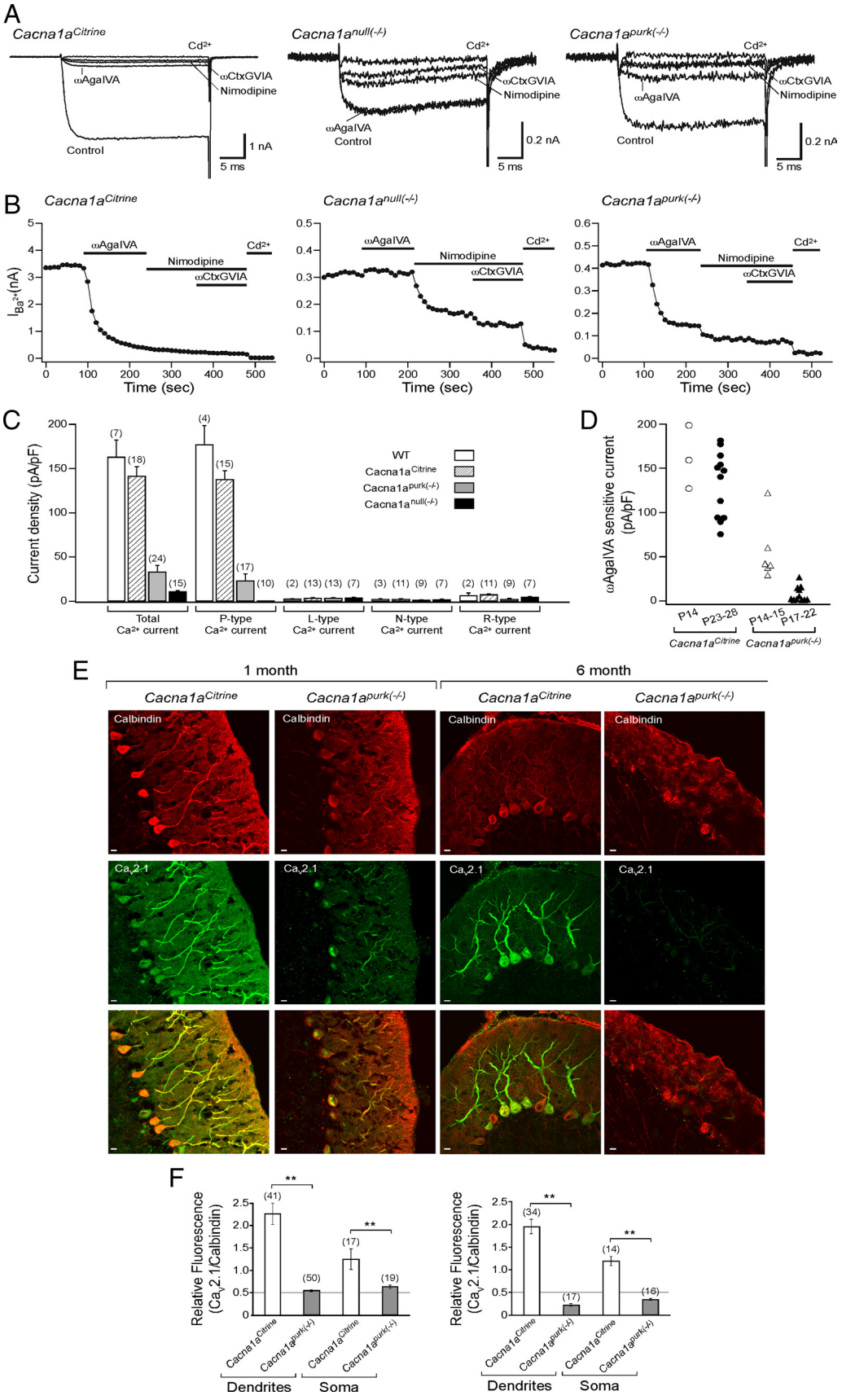

Figure 4. Loss of P/Q-type channel current and protein in *Cacna1a*$^{purk(-/-)}$ mice. ***A***, Representative whole-cell Ca^{2+} channel current evoked by 30 ms depolarization from −70 to −10 mV in dissociated PCs of *Cacna1a*^{Citrine}, *Cacna1a*$^{null(-/-)}$, and *Cacna1a*$^{purk(-/-)}$ mice, recorded before and after application of selective Ca^{2+} channel blockers, 0.1 μM ωAgaIVA (P/Q type), 1 μM ωCtxGVIA (N type), 1 μM nimodipine (L type), and Cd^{2+}. ***B***, Time course of inhibition of Ca^{2+} channel current by the indicated blockers (same cell as the top traces). ***C***, Bar graph showing Ca^{2+} channel current density and the contribution of P/Q-, N-, L-, and R-type currents to the total current (all experiments included) for *Cacna1a*^{Citrine}, *Cacna1a*$^{null(-/-)}$, and (*Figure legend continues.*)

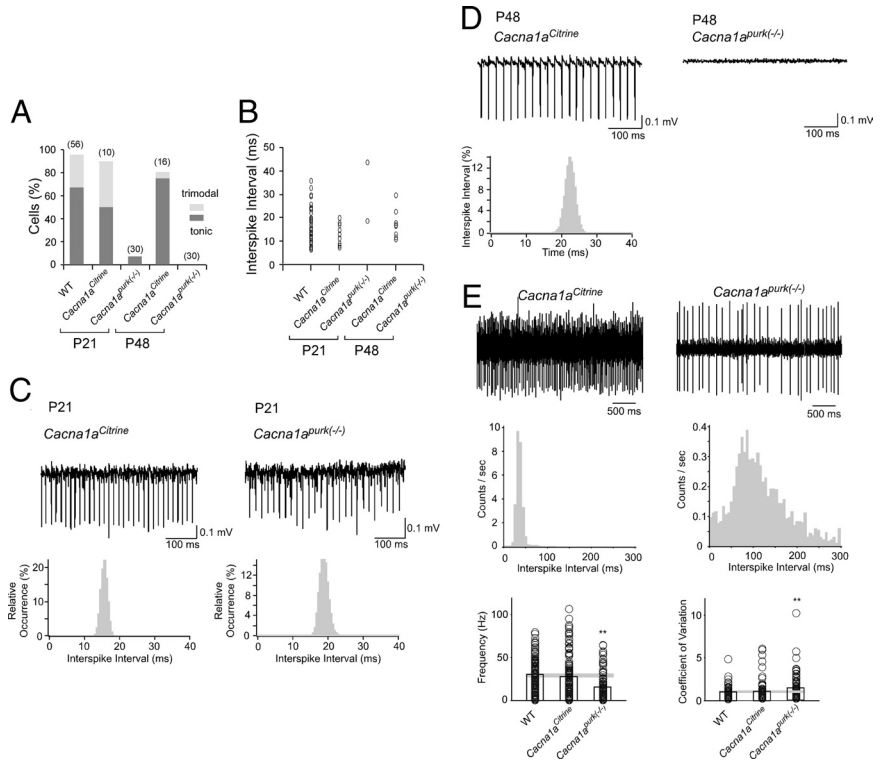

Figure 5. Altered activity of PCs and cerebellar neurons of *Cacna1a*$^{purk(-/-)}$ mice. ***A***, Bar graph of the percentage of spontaneously active PCs in WT mice at P21 and *Cacna1a*^{Citrine} and *Cacna1a*$^{purk(-/-)}$ mice at P21 and P48. Ninety-six percent ($n = 54$ of 56) of WT PCs exhibited spontaneous activity. Sixty-eight percent ($n = 38$ of 56) of cells exhibited tonic and 29% ($n = 16$ of 56) exhibited trimodal activity. Ninety percent ($n = 9$ of 10) of P21 *Cacna1a*^{Citrine} PCs fired spontaneously; 50% ($n = 5$ of 10) were tonic, and 40% ($n = 4$ of 10) were trimodal. Only 7% ($n = 2$ of 30) of P21 *Cacna1a*$^{purk(-/-)}$ PCs fired spontaneously; both cells were tonic. Eighty-one percent ($n = 13$ of 16) of P48 *Cacna1a*^{Citrine} PCs fired spontaneously; 75% ($n = 12$ of 16) were tonic, and 6% ($n = 1$ of 16) were trimodal. None ($n = 0$ of 30) of the *Cacna1a*$^{purk(-/-)}$ PCs fired spontaneously. ***B***, Distribution of interspike intervals for each experiment. Average interspike intervals were 16 ± 7 ms (WT), 13 ± 4 ms (P21 *Cacna1a*^{Citrine}), 31 ± 17 ms (P21 *Cacna1a*$^{purk(-/-)}$), and 18 ± 5 ms (P48 *Cacna1a*^{Citrine}). Interspike intervals for WT and P21 and P48 *Cacna1a*^{Citrine} PCs were not significantly different by one-way ANOVA ($F = 1.19$; $p < 0.31$). ***C***, Top, Sample traces of extracellular recordings of spontaneous tonic activity in P21 *Cacna1a*^{Citrine} (left) and *Cacna1a*$^{purk(-/-)}$ (right) PCs in cerebellar slices. Bottom, Distribution histograms of the interspike interval of spontaneous tonic activity over 200 s of recording in a single *Cacna1a*^{Citrine} PC (left) and in a single *Cacna1a*$^{purk(-/-)}$ PC (right). Sample traces and corresponding histograms are shown for the same cell. ***D***, Top, Sample traces of spontaneous tonic activity in a P48 *Cacna1a*^{Citrine} PC (left) and of inactivity in a P48 *Cacna1a*$^{purk(-/-)}$ (right) PC in cerebellar slices. Bottom, Distribution histogram of the interspike interval of spontaneous tonic activity over 200 s of recording in a single P48 *Cacna1a*^{Citrine} PC (left). ***E***, Cerebellar neurons of *Cacna1a*$^{purk(-/-)}$ mice fire more irregularly and with a lower frequency than those of control mice *in vivo*. Top, Example of spiking traces from cerebellar neurons recorded from *Cacna1a*^{Citrine} and *Cacna1a*$^{purk(-/-)}$ mice. Middle, Histogram of the interspike interval distribution of the recordings shown above. Bottom, Left, Distribution of the mean firing rates from WT, *Cacna1a*^{Citrine}, and *Cacna1a*$^{purk(-/-)}$ mice reveals that cerebellar neurons from *Cacna1a*$^{purk(-/-)}$ mice fire with a lower frequency. Right, Distribution of CV from WT, *Cacna1a*^{Citrine}, and *Cacna1a*$^{purk(-/-)}$ reveals that cerebellar neurons from *Cacna1a*$^{purk(-/-)}$ fire more irregularly. Bar graphs show distribution means. Recordings are from three *Cacna1a*^{Citrine}, three *Cacna1a*$^{purk(-/-)}$, and six WT mice (**$p < 0.01$, Mann–Whitney *U* test). The number in parentheses indicates the number of experiments.

1%, $n = 15$). In the genomic *Cacna1a* knock-out (*Cacna1a*^{null} mice), no ωAgaIVA-sensitive current was observed. In the conditional P/Q-type channel knock-out mice (*Cacna1a*$^{purk(-/-)}$), although the majority of Ca^{2+} current was ωAgaIVA sensitive (50 ± 9%; $n = 17$), the current density was one-third of the control *Cacna1a*^{Citrine} current density at P14–P15 (ωAgaIVA-sensitive current; *Cacna1a*^{Citrine}: 162 ± 21 pA/pF, $n = 3$; *Cacna1a*$^{purk(-/-)}$: 54 ± 14 pA/pF, $n = 6$). The ωAgaIVA-sensitive current further decreased to 5% of the control value at P17–P22 (*Cacna1a*^{Citrine}: 132 ± 11 pA/pF, $n = 12$; *Cacna1a*$^{purk(-/-)}$: 7 ± 3 pA/pF, $n = 11$). In 6 of the 11 cells from older (P17–P22) *Cacna1a*$^{purk(-/-)}$ mice, ωAgaIVA-sensitive current was not detected.

The decrease in P/Q-type current density is consistent with a reduction in P/Q-type channel number and protein. To investigate the localization of P/Q-type channels in PCs between *Cacna1a*^{Citrine} and *Cacna1a*$^{purk(-/-)}$ mice, cerebellar slices from 1- and 6-month-old mice were stained with specific antibodies against the P/Q-type channel and calbindin, a PC marker protein. As shown in Figure 4, *E* and *F*, P/Q-type channel antibody staining is significantly reduced in slices from the conditional P/Q-type channel knock-out mice compared with calbindin staining after 4 weeks of age. A further reduction in the intensity of P/Q-type channel staining is observed at 6 months of age. This loss of P/Q-type channel antibody staining in PCs from *Cacna1a*$^{purk(-/-)}$ mice is correlated with a 70% reduction in channel protein in the cerebellum after 6 months of age as demonstrated by Western blot (Fig. 3*F*). These results demonstrate that P/Q-type channel current and protein are drastically reduced by 3–4 weeks after birth in *Cacna1a*$^{purk(-/-)}$ mice.

Spontaneous activity patterns. Spontaneous action potential (AP) firing in PCs requires Ca^{2+} influx through P/Q-type channels (Womack and Khodakhah, 2004). We analyzed the activity of PCs in acute cerebellar slices under conditions in which fast excitatory and inhibitory synaptic inputs were blocked with CNQX and picrotoxin. Extracellular recordings of PCs from *Cacna1a*^{Citrine} mice revealed robust spontaneous activity at both P21 and P48 ($n = 10$ and 16, respectively) (Fig. 5*C*,*D*). As described previously in WT mice (Womack and Khodakhah, 2002; Walter et al., 2006), PCs from *Cacna1a*^{Citrine} mice fired either in a regular tonic pattern or in a trimodal pattern characterized by bursting, silent, and tonic activity (Fig. 5*A*). The interspike interval of spontaneous tonic firing activity was 13 ± 4 ms at P21 ($n = 10$) and 17 ± 5 ms ($n = 16$) at P48 and was not statistically different from that observed in WT mice (Fig. 5*B*). We found that 90% ($n = 9$ of 10) of PCs from P21 *Cacna1a*^{Citrine} mice and 81% ($n = 13$ of 16) of PCs from P48 *Cacna1a*^{Citrine} mice were spontaneously active (Fig. 5*A*). In contrast, in P21 *Cacna1a*$^{purk(-/-)}$ mice, only 2 of 30 cells demonstrated spontaneous activity in cerebellar slice recordings (Fig. 5*B*,*C*). At P48, we observed a complete loss of spontaneous activity as none of the PCs displayed AP firing even after 30 min of recording ($n = 0$ of 30) (Fig. 5*B*,*D*). Thus, PCs from *Cacna1a*$^{purk(-/-)}$ mice lose their capacity to fire APs spontaneously in cerebellar slices between 3 and 7 weeks after birth. To evaluate whether the loss of P/Q-type channels in PCs affect the firing properties of cerebellar neurons in the living animal, we performed *in vivo* recordings in the PC layer of anesthetized mice (Fig. 5*E*). We combined recordings of all neurons with simple spikes within the proximity of putative PCs (given by the electrode position), because of the difficulty in detecting complex spikes, and the decreased frequency and increased CV in *Cacna1a*$^{purk(-/-)}$ mice. We found that neurons within the PC layer of *Cacna1a*$^{purk(-/-)}$ mice fire

←

(*Figure legend continued.*) *Cacna1a*$^{purk(-/-[supi])}$ mice. The total Ca^{2+} channel current density (first value) was higher than the P/Q-type current density (second value) within PC (in pA/pF): WT, 187.2 ± 19.3 ($n = 4$) vs 177.3 ± 21.4 ($n = 4$); *Cacna1a*^{Citrine}, 150.9 ± 9.8 ($n = 15$) vs 137.9 ± 9.7 ($n = 15$); *Cacna1a*$^{null(-/-)}$, 32.6 ± 8.8 ($n = 17$) vs 23.5 ± 7.5 ($n = 17$); *Cacna1a*$^{purk(-/-)}$, 11.4 ± 1.3 ($n = 10$) vs 0.3 ± 0.2 ($n = 10$). ***E***, Comparison of the protein expression of P/Q-type channels in PCs between *Cacna1a*^{Citrine} and *Cacna1a*$^{purk(-/-)}$ mice at 1 and 6 months of age. ***F***, Quantification of the relative fluorescence of the secondary antibody against P/Q-type channels relative to the fluorescence of the secondary antibody against Calbindin-D for *Cacna1a*^{Citrine} and *Cacna1a*$^{purk(-/-)}$ mice at 1 and 6 months of age. **$p < 0.01$. Scale bar, 10 μm. The number in parentheses indicates the number of experiments.

with a lower frequency and reveal a higher CV (15.2 ± 1.5 Hz and 1.43 ± 0.12; $n = 112$) compared with WT (30.5 ± 1.9 Hz and 0.96 ± 0.06; $n = 115$) and *Cacna1a*^{Citrine} (27.4 ± 2.2 Hz and 1.08 ± 0.08 ($n = 137$) mice older than 6 months of age. Thus, our results indicate that removal of P/Q-type channels from PCs reduces the neuronal activity and the precision of firing of presumed PCs in living mice.

Alteration in Ca^{2+} channel dependence and reduction of transmitter release at PC deep cerebellar nucleus synapses. To determine whether P/Q-type channel reduction alters release at PC axon terminals, we analyzed the contribution of P/Q-type currents to evoked synaptic transmission in the deep cerebellar nucleus (DCN). Evoked GABAergic IPSCs were recorded in DCN neurons. We found that IPSCs were completely blocked by application of ωAgaIVA in *Cacna1a*^{Citrine} cerebellar slices (Fig. 6*A*,*C*). In contrast, ωAgaIVA did block synaptic transmission only by <10% in *Cacna1a*$^{purk(-/-)}$ mice. However, IPSCs were reduced by ~60% after application of the N-type channel blocker ωCtxGVIA (Fig. 6*B*,*D*). IPSCs were completely blocked by the $GABA_A$ receptor antagonist Gabazine (10 μM; data not shown). The loss of P/Q-type channels at the presynaptic terminal was correlated with a fivefold reduction in the evoked IPSC size. Averaged IPSC amplitude was 2.53 ± 0.38 nA ($n = 7$) in *Cacna1a*^{Citrine} mice and 0.47 ± 0.1 nA ($n = 6$) in the *Cacna1a*$^{purk(-/-)}$ mice 2–3 weeks of age. These results suggest that synaptic transmission at PC terminals of *Cacna1a*$^{purk(-/-)}$ mice in the DCN is reduced but persists in the absence of P/Q-type channels, relying mainly on N-type channel-mediated exocytosis.

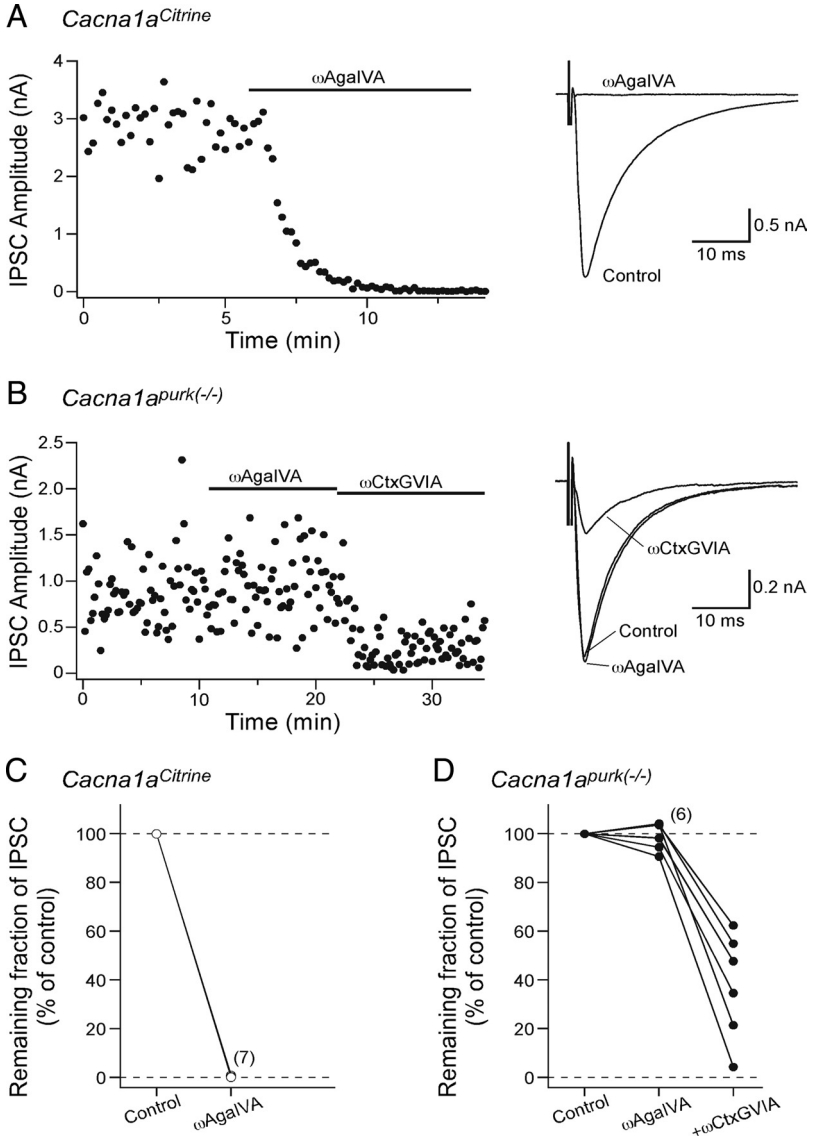

Figure 6. Loss of P/Q-type channel contribution for transmitter release at PC to deep cerebellar nucleus neuron synapses in *Cacna1a*$^{purk(-/-)}$ mice. ***A***, ***B***, Time course of inhibition of IPSC by Ca^{2+} channel blockers, recorded in DCN neurons of 15- to 18-d-old *Cacna1a*^{Citrine} (***A***) and *Cacna1a*$^{purk(-/-)}$ (***B***) mice. A total of 0.2 μM ωAgaIVA and subsequently 3 μM ωCtxGVIA were applied. Right, Averaged IPSCs obtained in the presence of the blockers. ***C***, ***D***, Plots showing the remaining fraction of IPSCs after blockade by the indicated blockers for *Cacna1a*^{Citrine} (***C***) and *Cacna1a*$^{purk(-/-)}$ (***D***) mice. Plots are connected for the same cells.

Ataxia

We next analyzed the behavioral consequences of the conditional knock-out of P/Q-type channels in PCs. *Cacna1a*$^{purk(-/-)}$ mice develop a mild to severe ataxic gait after 2 weeks of age. The ataxia can be easily visualized in a footprint assay of spontaneous gait that demonstrates a difference in stride length and forelimb/hindlimb overlap (print positions) of 3-month-old *Cacna1a*$^{purk(-/-)}$ mice compared with their *Cacna1a*^{Citrine} littermates (Table 1). To quantify their motor deficit, we performed additional tests, including the rotarod, vertical pole, inclined screen, grip strength, and Basso Mouse Scale (BMS) evaluation with 3- to 6-month-old mice. *Cacna1a*$^{purk(-/-)}$ mice performed extremely poorly on the rotarod test. While *Cacna1a*^{Citrine} control mice were able to stay on the rotorod for an average of 100 s at a turning speed of up to 14 rpm and improved their performance during a 3 d trial period to 160 s at a final turning speed of 20 rpm, littermate *Cacna1a*$^{purk(-/-)}$ mice fell off the rod after 20 s at a turning rate of 5 rpm and did not improve their performance during the 3 d trial period (Fig. 7*B*). Similar deficits were observed on the inclined screen (Fig. 7*C*) and vertical pole (Fig. 7*D*) tests. *Cacna1a*^{Citrine} mice needed 27 and 32 s, respectively, for a 60° and a 90° incline, whereas the PC P/Q-type channel knock-down mice needed approximately twice that time to reach the platform (Fig. 7*C*).

Table 1. Footprint analysis

	Cacana1a^{Citrine}	*n*	*Cacana1a*$^{purk(-/-)}$	*n*
Stride length				
Right forelimb	40.33 ± 2.26	3	13.8 ± 2.4	3
Left forelimb	37.03 ± 3.29	3	13.51 ± 2.03	3
Right hindlimb	40.33 ± 2.19	3	13.9 ± 2.61	3
Left hindlimb	40.02 ± 2.5	3	11.79 ± 2.06	3
Print positions[a]				
RF⟶RH	1.88 ± 1.24	3	14.98 ± 9.20	3
LF⟶LH	3.45 ± 1.84	3	12.55 ± 7.82	3

[a]Print positions is forelimb (F)/hindlimb (H)overlap. R, Right; L, left. Stride length is in millimeters. Data represent mean ± SEM.

In addition, *Cacna1a*$^{purk(-/-)}$ mice were not able to cling to the pole and were scored with the maximal time of 120 s. We used a modified version of the BMS for locomotion as a quantitative measure for the severity of ataxia (Basso et al., 2006).

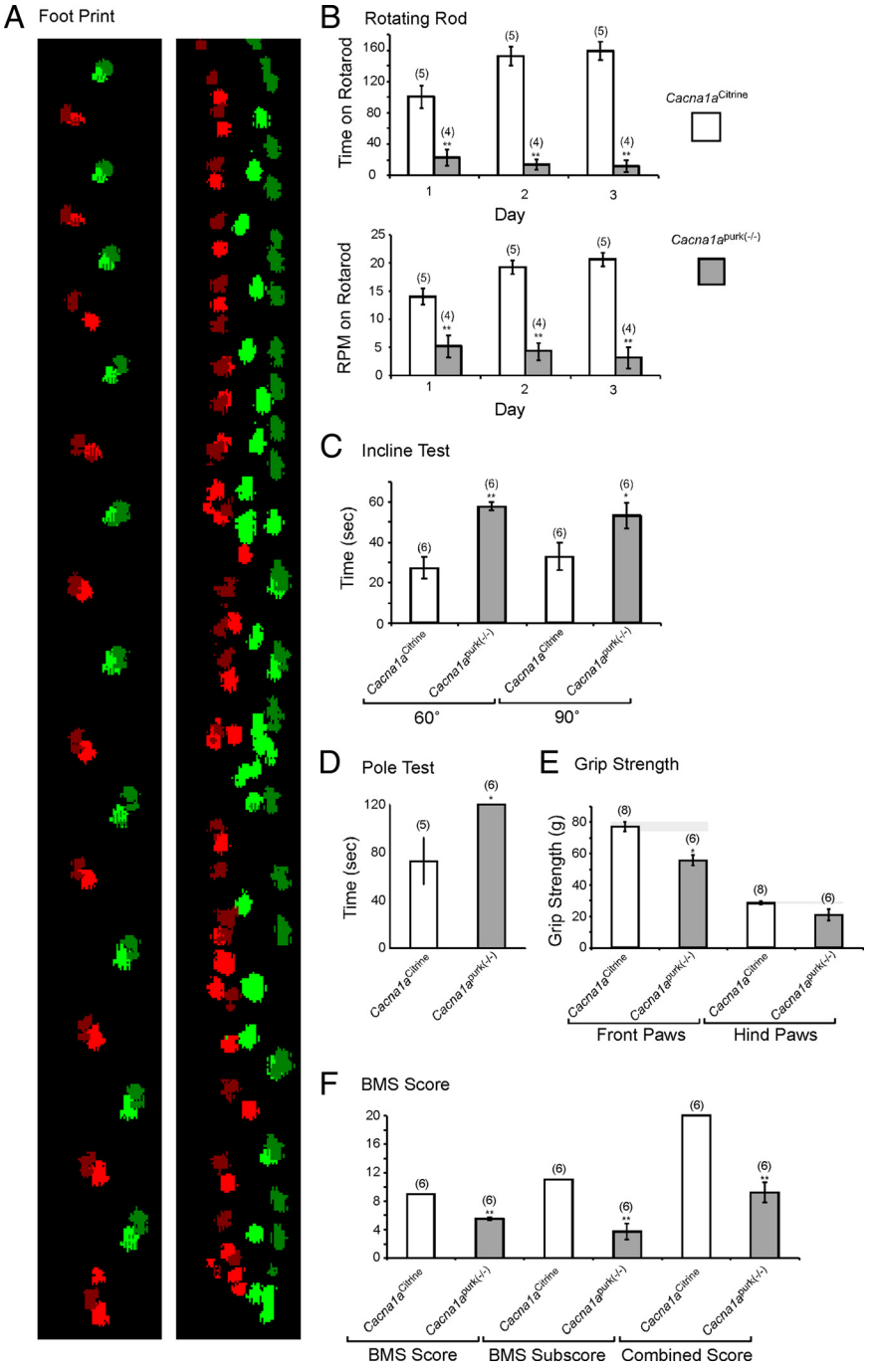

Figure 7. Behavioral analysis of *Cacna1a*$^{purk(-/-)}$ mice. Comparisons between *Cacna1a*^{Citrine} and *Cacna1a*$^{purk(-/-)}$ mice of footprint (***A***), rotarod (***B***), incline screen test (***C***), pole test (***D***), grip strength of the front paws and hind paws (***E***), and BMS scores (***F***). Statistical significance in all behavior experiments was evaluated with ANOVA. *$p < 0.05$; **$p < 0.01$. Standard errors are mean ± SEM. The number in parentheses indicates the number of experiments.

The *Cacna1a*$^{purk(-/-)}$ mice received a BMS score of 5.5, consistent with frequent plantar stepping and some coordination between the forelimb and the hindlimb step (Fig. 7*F*). Although stride length between forelimb and hindlimb was reduced, *Cacna1a*$^{purk(-/-)}$ were still able to move with a consistent speed and distance as seen in the footprints (Fig. 7*A* and Table 1). To determine whether the loss of P/Q-type channels in PCs also reduced coordinated motor strength, we performed a grip strength assay and detected differences in the forepaws but not hindpaws (Fig. 7*E*). This may partially reflect a fine motor grasp deficit rather than a difference in muscle strength, since *Cacna1a*$^{purk(-/-)}$ mice had difficulties coordinating their forepaw grip.

Analysis of dyskinesias and thalamocortical absence seizures

As early as 3 weeks after birth, *Cacna1a*$^{purk(-/-)}$ mice develop spontaneous episodes of paroxysmal dyskinesia (Fig. 8*A* and Table 2; supplemental Movie 4, available at www.jneurosci.org as supplemental material). These unprovoked events consist of sustained axial dystonia and repetitive clonic limb movements without changes in the cortical EEG as described in the *tottering* and *leaner* alleles of mice with spontaneous *Cacna1a* mutations (Noebels and Sidman, 1979; Khan and Jinnah, 2002). The mean frequency of spontaneous dystonic attacks within a 24 h period was 2.3 ± 4.1 ($n = 18$), and the episodes showed a typical duration of about 40 min. These dyskinesias could also be induced in adult mice (3–18 months old) by stress or chemicals, such as a new environment, cage transport, short restraint, or administration of caffeine and alcohol (Table 2). Finally, to fully evaluate the phenotypic triad characteristic of P/Q-type loss of function, we looked for generalized, nonconvulsive spike-wave neocortical discharges by performing prolonged video EEG monitoring in awake, behaving mutant mice at 1–4 months of age. Surprisingly, we found that the *purky* mice show stereotyped 6–7 spikes/s generalized spike-wave seizure discharges accompanied by behavioral arrest identical to those in genomic *Cacna1a* mutants (Fig. 8*B*), despite the lack of obvious differences in the distribution of P/Q-type channels in thalamic relay or parvalbumin-positive reticular neurons between *Cacna1a*^{Citrine} and *Cacna1a*$^{purk(-/-)}$ mice (Fig. 8*C*). This pattern of seizure activity has long been considered to reflect alterations in the interplay between neurons in neocortex, reticular, and thalamic relay nuclei. We therefore analyzed P/Q-type channel-mediated GABAergic synaptic transmission at the nucleus reticularis of the thalamus (nRT). These neurons send inhibitory projections into the thalamic relay cells and undergo a developmental shift between N-type and P/Q-type channels between P10 and P19 (Iwasaki et al., 2000). We recorded the GABAergic IPSCs from thalamocortical relay neurons in the laterodorsal thalamic nucleus after stimulation of the nRT. We found that at P19–P21, synaptic transmitter release is uniformly and almost completely blocked by the P/Q-type channel blocker ωAgaIVA in *Cacna1a*^{Citrine} mice (91.5 ± 3.7%; $n = 7$) (Fig. 8*E*). In contrast, in *Cacna1a*$^{purk(-/-)}$ mice we found a high degree of variability in

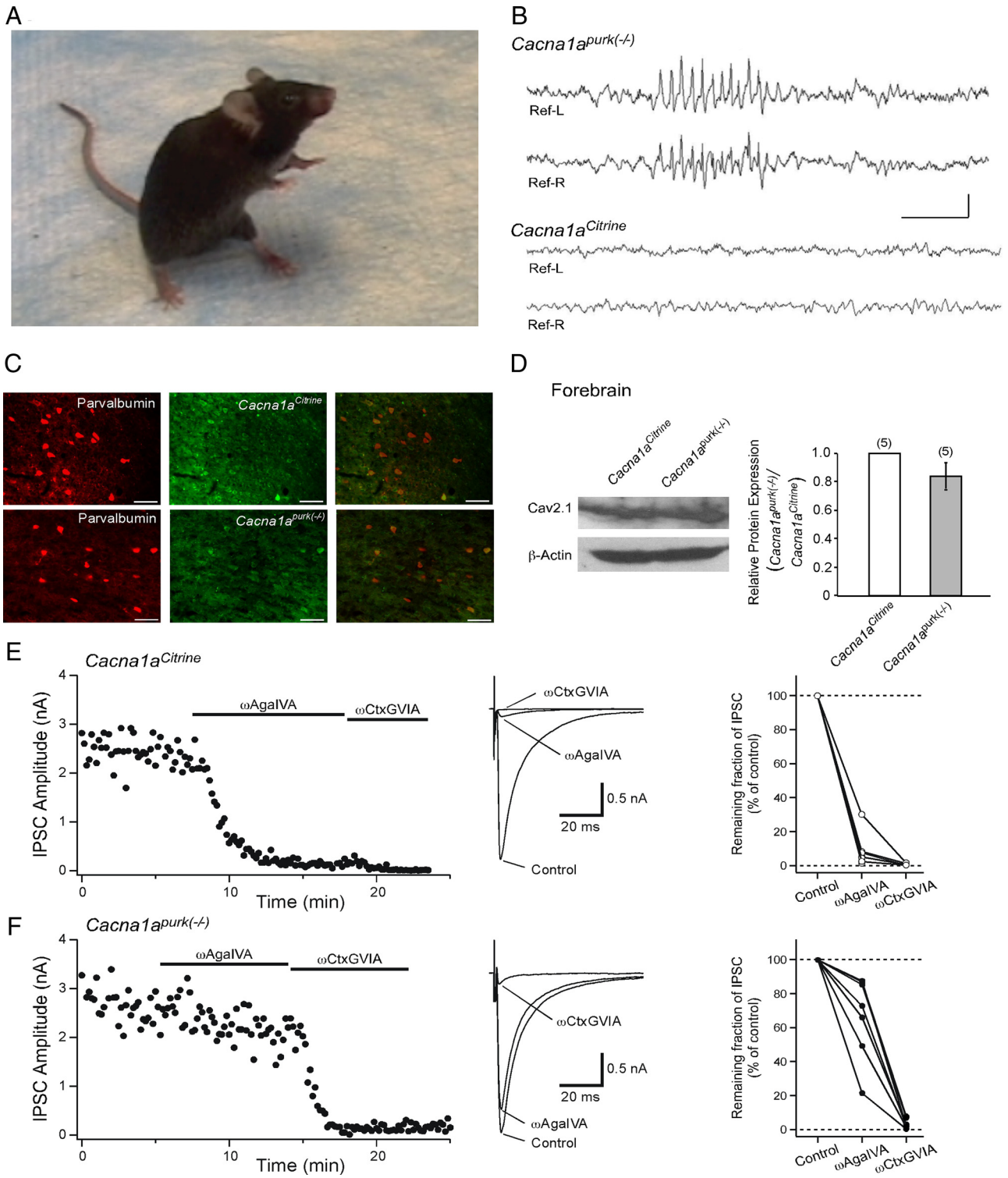

Figure 8. Cacna1a $^{purk(-/-)}$ mice develop paroxysmal dyskinesia and absence epilepsy. ***A***, Nine-month-old male *Cacna1a*$^{purk(-/-)}$ mouse during an episode of motor dyskinesia. The picture was taken from supplemental Movie 4 (available at www.jneurosci.org as supplemental material) and illustrates the typical exaggerated truncal posture with forepaw clonus. ***B***, Spontaneous bilateral generalized 6–7 s spike discharge in cortical EEG recording from left (L) and right (R) hemispheres accompanied by behavioral arrest in an awake *Cacna1a*$^{purk(-/-)}$ mutant. Abnormal discharges were never observed in control *Cacna1a*^{Citrine} mice. Calibration: 1 s, 300 μV. ***C***, Comparison of P/Q-type channel staining (green) in parvalbumin-positive neurons (red) showing similar evidence of P/Q-type expression in thalamic neurons of 6-week-old *Cacna1a*^{Citrine} and *Cacna1a*$^{purk(-/-)}$ mice. Scale bar, 40 μm. ***D***, Right, Western blot analysis of forebrain homogenates from adult *Cacna1a*^{Citrine} and *Cacna1a*$^{purk(-/-)}$ mouse brains. Left, Relative protein expression of Cacna1A and β-actin as a loading control was determined. ***E***, ***F***, Alteration of P/Q-type channel contribution for synaptic transmission from GABAergic interneuron to thalamic nuclei neurons in *Cacna1a*$^{purk(-/-)}$ mice compared with *Cacna1a*^{Citrine} mice. Left, Time course of inhibition of IPSC by Ca^{2+} channel blockers recorded in LD thalamic nucleus neurons of *Cacna1a*^{Citrine} (***E***) and *Cacna1a*$^{purk(-/-)}$ (***F***) mice. A total of 0.2 μM ωAgaIVA and subsequently 1 μM ωCtxGVIA were applied. Middle, Example traces of IPSCs before and after application of the indicated Ca^{2+} channel blockers for *Cacna1a*^{Citrine} (***E***) and *Cacna1a*$^{purk(-/-)}$ (***F***) mice. Right, Plots showing the remaining fraction of IPSCs after blocked by the indicated blockers for *Cacna1a*^{Citrine} (***E***) and *Cacna1a*$^{purk(-/-)}$ (***F***) mice. Plots are connected for the same cells. The number in parentheses indicates the number of experiments.

Table 2. Frequency and duration of spontaneous and induced dyskinesias

Treatment	Mouse line	*n*	Seizure (%)	Seizure time (min)
Cage change	*Cacna1a*^{Citrine}	27	0	
	Cacna1a$^{purk(-/-)}$	14	28.6 ± 6	46.5 ± 5.3
Cage transport	*Cacna1a*^{Citrine}	27	0	
	Cacna1a$^{purk(-/-)}$	14	21.4 ± 4.5	38.3 ± 5.1
Short restraint	*Cacna1a*^{Citrine}	27	0	
	Cacna1a$^{purk(-/-)}$	14	57.1 ± 6.9	37.0 ± 4.6
Saline	*Cacna1a*^{Citrine}	22	0	
	Cacna1a$^{purk(-/-)}$	14	57 ± 8.4	49.0 ± 8.9
Caffeine	*Cacna1a*^{Citrine}	11	0	
	Cacna1a$^{purk(-/-)}$	13	69.2 ± 5.8	33.2 ± 5.4
Ethanol	*Cacna1a*^{Citrine}	11	0	
	Cacna1a$^{purk(-/-)}$	13	100	55.5 ± 4.2

Behavioral studies were performed according to the study by Fureman et al. (2002). Data represent the percentage of mice that had a dyskinetic episode per mouse group and the average duration of the dyskinesia per group. Data represent mean ± SEM.

P/Q-type channel-dependent IPSCs, ranging from 10 to 80% (32.9 ± 9.2%; $n = 7$) suggesting a "leaky" partial deletion of *Cacna1a* in nRT (Fig. 8*F*). There was no significant change in the amplitude of evoked IPSCs (*Cacna1a*^{Citrine}: 3.46 ± 0.53 nA; $n = 7$) and *Cacna1a*$^{purk(-/-)}$: 2.17 ± 0.57 nA; $n = 7$). To determine whether these results could be explained by either an alteration in cerebellar output regulating the development of thalamocortical projections or a small residual expression of Cre recombinase in GABAergic interneurons driven by the PCP2 Cre promoter, leading to the deletion of the P/Q-type channel outside of the cerebellum, we compared the P/Q-type channel protein levels of the adult forebrain. We found that the protein level in *Cacna1a*$^{purk(-/-)}$ mice is reduced by 16% compared with *Cacna1a*^{Citrine} mice (84 ± 9%; $n = 5$) (Fig. 8*D*). This result suggests that a sparse expression of Cre recombinase in the PCP2-Cre mouse line within the thalamus and probably elsewhere in the brain can likely account for the abnormal thalamocortical signaling in *purky* mice.

Discussion

Visualization of neuronal membrane P/Q-type channels

We engineered a new mouse model allowing the visualization and cell-type-specific knockdown of P/Q-type channels and demonstrate that Citrine-tagged P/Q-type channels remain functional and can be detected with GFP antibodies. We tagged the channel in the first exon of the *Cacna1a* gene and flanked the Citrine with loxP sites for the Cre-recombinase-mediated excision of exon 1. The endogenous GFP-tagged channel retains WT function in cerebellar PCs, as evidenced by unaltered cellular firing properties and the lack of a neurobehavioral phenotype in these mice. To reduce the number of electroporations and time in culture, we introduced our *Cacna1a*-Citrine targeting vector into ES cells containing PrmCre, allowing knock-in of a floxed Citrine of *Cacna1a* in the first generation of mice. The phenotype of these PrmCre-mediated knock-out mice resembled other P/Q-type channel mutations where exon 3 was deleted (Jun et al., 1999; Fletcher et al., 2001; Todorov et al., 2006). This new construct should prove valuable in future genotype–phenotype analyses aimed at dissecting the role of Cav2.1 function in a variety of Cre-expressing lines targeting specific CNS networks.

PC predominant knockdown of P/Q-type channels

We selected the Cre promoter line Tg$^{PCP2\text{-}cre}$ to conditionally ablate P/Q currents in these cells. This line reveals high specific Cre activity in PCs in cerebellar folia and very low Cre activity in retinal bipolar cells and other brain regions (Barski et al., 2000). Cre activity in the cerebellum is first observed at P6 and fully established within 2–3 weeks after birth.

We first analyzed the loss of P/Q-type current in dissociated PCs from 2- to 3-week-old *purky* mice. The *purky* mice showed a graded reduction in ωAgaIVA-sensitive Ca^{2+} current density; 33% of this current remained at 2 weeks, and only 5% of current remained after 3 weeks of age, suggesting that either the P/Q-type channel turnover rate or the PCP2 promoter upregulation is slow. In contrast, the PrmCre knock-out of $Ca_v2.1$, where the channel is deleted immediately, shows no P/Q-type current in PCs. The residual Ca^{2+} current is primarily attributable to N-type and L-type currents observed previously in other *Cacna1a* mutant mouse lines (Jun et al., 1999; Qian and Noebels, 2000).

The loss of P/Q-type current reflected the lower channel protein expression in PCs from *Cacna1a*$^{purk(-/-)}$ mice. P/Q-type channel staining in *Cacna1a*$^{purk(-/-)}$ slices was reduced by 50–80% at the soma/dendrites after 1 month and by 70–90% after 6 months of age compared with their *Cacna1a*^{Citrine} littermates. The very weak immunofluorescence detected in older animals is likely caused by nonspecific background staining; however, we cannot exclude that a low level of P/Q-type channel remains. We saw no obvious changes in PC number from *Cacna1a*$^{purk(-/-)}$ mice at 3 month of age; however, the cerebellar cortical molecular layer appears abnormally thin when compared with *Cacna1a*^{Citrine} mice. A careful investigation of changes in PC number and dendritic morphology will be needed to reveal how *Cacna1a*$^{purk(-/-)}$ mice compare with other ataxic P/Q-type Ca^{2+} channel mouse models (Rhyu et al., 1999a,b; Hoebeek et al., 2008).

The physiological consequence of reduced P/Q-type current in PCs from cerebellar slices is the absence of spontaneous activity in slice recordings, which has also been observed in the *Cacna2d2* mutant mouse ducky^{2J} (Donato et al., 2006). Our results agree with previous studies showing that inhibition of VGCCs and/or P/Q-type channels blocks spontaneous activity (Womack and Khodakhah, 2004) and is important for PC firing (Swensen and Bean, 2003; Khaliq and Raman, 2006; Levin et al., 2006). P/Q-type channels in PCs are coupled to Ca^{2+}-activated K^+ channels (Womack et al., 2004), which also regulate intrinsic repetitive AP firing properties (Llinas and Sugimori, 1980a,b; Tank et al., 1988; Womack et al., 2004; Walter et al., 2006). Additionally, we found reduced firing frequency and increased CV of cerebellar neurons in *purky* mice. A decrease in the precision of PC firing has also been detected in other P/Q mutant alleles, such as *ducky*, *leaner*, and *tottering,* and has been suggested to contribute to the ataxic phenotype (Hoebeek et al., 2005; Walter et al., 2006). We also observed low-frequency oscillations in some cerebellar neurons from *purky* (data not shown) as described recently in *tottering* (Chen et al., 2009). We analyzed the functional consequences of PC-specific loss of P/Q-type channels at the presynaptic terminal and found that after 3 weeks of age, severely ataxic mice completely lost most of their sensitivity to the P/Q-type channel blocker ωAgaIVA, which correlated with a reduction in IPSC amplitude. The remaining synaptic transmission relies mainly on N-type channels. A similar finding has been reported at central synapses in *tottering* mice (Qian and Noebels, 2000; Inchauspe et al., 2007).

Targeted postnatal PC knock-out of P/Q-type channels replicates genomic deficiency phenotypes

Although an ataxic phenotype is predicted for inherited *Cacna1a* channelopathy, a critical period for this phenotype has never been established. This neurological deficit, typically appearing in mutant mice at 2–4 weeks of age, might be determined by either

an impairment of central motor pathways beginning in embryonic development, an early signaling defect coinciding with postnatal cerebellar development, or a dysfunction that commences once cerebellar development is essentially complete during the juvenile period. We found that delaying the ablation of P/Q-type channels until the second postnatal week produced a deficit in cerebellar function comparable to those seen in inherited models of *Cacna1a* deficiency. In addition, the delayed loss of P/Q-type channels in PCs results in similar episodes of dyskinesia (supplemental Video 4, available at www.jneurosci.org as supplemental material). Identical episodes of dyskinesia (paroxysmal dystonia with clonic limb shaking) are also observed in other P/Q-type channel loss-of-function mutants such as *tottering, ducky*, and *lethargic* (Noebels and Sidman, 1979), and their exact neural mechanism is unknown (Fletcher et al., 1996; Burgess et al., 1997; Fletcher and Frankel, 1999; Barclay et al., 2001; Khan and Jinnah, 2002; Pietrobon, 2005). Cerebellar pathways are involved (Pizoli et al., 2002), and the episodes are eliminated when PCs are genetically removed (Campbell et al., 1999); however, their dependence on normal PC signaling patterns has not been previously demonstrated.

An unexpected phenotype in *Cacna1a*$^{purk(-/-)}$ mice was the appearance of generalized absence epilepsy, since the brain regions considered critical for the generation of thalamocortical absence seizures include the sensorimotor areas of the neocortex and associated reticular and thalamic relay nuclei but not cerebellar circuitry (Steriade and Llinas, 1988; Buzsaki, 1991; Timofeev and Steriade, 2004; Meeren et al., 2005). We considered several possible explanations for this thalamocortical network excitability phenotype in *purky* mice. First, since small changes in GABAergic transmission have been shown sufficient to induce abnormal discharges in thalamocortical networks (Sohal and Huguenard, 2003), one possibility is that the spike-wave discharges reflect slight defects in forebrain inhibitory network synchronization because of leakage of the PCP2/L7 promoter, impairing release at a small population of critical synapses in neocortex and thalamus (Barski et al., 2000). In agreement with this, we found a change in the P/Q-type channel dependence of GABAergic transmitter release in inhibitory interneurons and a 16% reduction in forebrain P/Q-type channel protein levels. The results suggest that residual nonspecific Cre activity outside the cerebellar PCs reduces forebrain P/Q-type channels, consistent with a recent finding that other transgenic PCP2-Cre-driver lines reveal scattered Cre-mediated dtTomato expression in the forebrain (Madisen et al., 2010). However, it remains surprising that the synchronization phenotype can arise from this small reduction in P/Q-type channels, since mice heterozygous for *tottering*, *lethargic*, and *ducky* mutations, as well as juvenile mice haploinsufficient for the *Cacna1a* locus that lack 50% of the normal population of P/Q-type channels, are phenotypically normal without evidence of cortical discharges (Pietrobon, 2010). An additional possibility is that normal oscillatory patterns in thalamocortical circuitry could depend on early cerebellar input to thalamic nuclei. The decreased output of PCs in *purky* mice reduces inhibition of neurons in deep cerebellar nuclei; if this disinhibition increases the output of the cerebellar projection to the thalamus, it could contribute to a developmental alteration in firing properties in adult thalamocortical circuitry contributing to the epileptic phenotype, including changes in T-type Ca^{2+} current densities in thalamic neurons or plasticity changes within excitatory or inhibitory neurons in the thalamocortical network. These mechanisms could be induced indirectly by changes in the thalamic input via abnormal cerebellar output activity patterns or directly via sparse, random loss of the P/Q-type channel within the thalamocortical circuit itself.

Our data demonstrate that a delayed, postnatal loss of P/Q-type channels throughout the brain recreates the three major neurological deficits of ataxia, dyskinesia, and absence epilepsy. Since the developmental onset of Ca^{2+} channelopathy has never before been correlated with the extent and severity of the neurological phenotype, the full spectrum of deficits displayed in the *purky* mouse show that the disorder does not depend on dysfunctional prenatal, or even precerebellar, development but results from altered signaling patterns and impaired neurotransmission beginning as late as infancy. This finding is the first to define a delayed therapeutic window for the reversibility of inherited Ca^{2+} ion channel disorders.

References

Barclay J, Balaguero N, Mione M, Ackerman SL, Letts VA, Brodbeck J, Canti C, Meir A, Page KM, Kusumi K, Perez-Reyes E, Lander ES, Frankel WN, Gardiner RM, Dolphin AC, Rees M (2001) Ducky mouse phenotype of epilepsy and ataxia is associated with mutations in the Cacna2d2 gene and decreased calcium channel current in cerebellar Purkinje cells. J Neurosci 21:6095–6104.

Barski JJ, Dethleffsen K, Meyer M (2000) Cre recombinase expression in cerebellar Purkinje cells. Genesis 28:93–98.

Basso DM, Fisher LC, Anderson AJ, Jakeman LB, McTigue DM, Popovich PG (2006) Basso Mouse Scale for locomotion detects differences in recovery after spinal cord injury in five common mouse strains. J Neurotrauma 23:635–659.

Brodbeck J, Davies A, Courtney JM, Meir A, Balaguero N, Canti C, Moss FJ, Page KM, Pratt WS, Hunt SP, Barclay J, Rees M, Dolphin AC (2002) The ducky mutation in Cacna2d2 results in altered Purkinje cell morphology and is associated with the expression of a truncated alpha 2 delta-2 protein with abnormal function. J Biol Chem 277:7684–7693.

Burgess DL, Noebels JL (1999) Single gene defects in mice: the role of voltage-dependent calcium channels in absence models. Epilepsy Res 36:111–122.

Burgess DL, Jones JM, Meisler MH, Noebels JL (1997) Mutation of the Ca2+ channel beta subunit gene Cchb4 is associated with ataxia and seizures in the lethargic (lh) mouse. Cell 88:385–392.

Burright EN, Clark HB, Servadio A, Matilla T, Feddersen RM, Yunis WS, Duvick LA, Zoghbi HY, Orr HT (1995) SCA1 transgenic mice: a model for neurodegeneration caused by an expanded CAG trinucleotide repeat. Cell 82:937–948.

Buzsaki G (1991) The thalamic clock: emergent network properties. Neuroscience 41:351–364.

Campbell DB, North JB, Hess EJ (1999) Tottering mouse motor dysfunction is abolished on the Purkinje cell degeneration (pcd) mutant background. Exp Neurol 160:268–278.

Catterall WA (2000) Structure and regulation of voltage-gated Ca2+ channels. Annu Rev Cell Dev Biol 16:521–555.

Catterall WA, Few AP (2008) Calcium channel regulation and presynaptic plasticity. Neuron 59:882–901.

Chen G, Popa LS, Wang X, Gao W, Barnes J, Hendrix CM, Hess EJ, Ebner TJ (2009) Low-frequency oscillations in the cerebellar cortex of the tottering mouse. J Neurophysiol 101:234–245.

Donato R, Page KM, Koch D, Nieto-Rostro M, Foucault I, Davies A, Wilkinson T, Rees M, Edwards FA, Dolphin AC (2006) The ducky(2J) mutation in Cacna2d2 results in reduced spontaneous Purkinje cell activity and altered gene expression. J Neurosci 26:12576–12586.

Dunlap K, Luebke JI, Turner TJ (1995) Exocytotic Ca2+ channels in mammalian central neurons. Trends Neurosci 18:89–98.

Edwards FA, Konnerth A, Sakmann B, Takahashi T (1989) A thin slice preparation for patch clamp recordings from neurones of the mammalian central nervous system. Pflugers Arch 414:600–612.

Feil R, Hartmann J, Luo C, Wolfsgruber W, Schilling K, Feil S, Barski JJ, Meyer M, Konnerth A, De Zeeuw CI, Hofmann F (2003) Impairment of LTD and cerebellar learning by Purkinje cell-specific ablation of cGMP-dependent protein kinase I. J Cell Biol 163:295–302.

Fletcher CF, Frankel WN (1999) Ataxic mouse mutants and molecular mechanisms of absence epilepsy. Hum Mol Genet 8:1907–1912.

Fletcher CF, Lutz CM, O'Sullivan TN, Shaughnessy JDJ, Hawkes R, Frankel WN, Copeland NG, Jenkins NA (1996) Absence epilepsy in tottering mutant mice is associated with calcium channel defects. Cell 87:607–617.

Fletcher CF, Tottene A, Lennon VA, Wilson SM, Dubel SJ, Paylor R, Hosford DA, Tessarollo L, McEnery MW, Pietrobon D, Copeland NG, Jenkins NA (2001) Dystonia and cerebellar atrophy in Cacna1a null mice lacking P/Q calcium channel activity. FASEB J 15:1288–1290.

Fureman BE, Jinnah HA, Hess EJ (2002) Triggers of paroxysmal dyskinesia in the calcium channel mouse mutant tottering. Pharmacol Biochem Behav 73:631–637.

Han J, Mark MD, Li X, Xie M, Waka S, Rettig J, Herlitze S (2006) RGS2 determines short-term synaptic plasticity in hippocampal neurons by regulating Gi/o-mediated inhibition of presynaptic Ca2+ channels. Neuron 51:575–586.

Hartmann J, Konnerth A (2005) Determinants of postsynaptic Ca2+ signaling in Purkinje neurons. Cell Calcium 37:459–466.

Heikal AA, Hess ST, Baird GS, Tsien RY, Webb WW (2000) Molecular spectroscopy and dynamics of intrinsically fluorescent proteins: coral red (dsRed) and yellow (Citrine). Proc Natl Acad Sci U S A 97:11996–12001.

Herlitze S, Xie M, Jan J, Hümmer A, Melnik-Martinez KV, Moreno RL, Mark MD (2003) Targeting mechanisms of high voltage-activated Ca2+ channels. J Bioenerg Biomembr 35:621–637.

Hoebeek FE, Stahl JS, van Alphen AM, Schonewille M, Luo C, Rutteman M, van den Maagdenberg AM, Molenaar PC, Goossens HH, Frens MA, De Zeeuw CI (2005) Increased noise level of purkinje cell activities minimizes impact of their modulation during sensorimotor control. Neuron 45:953–965.

Hoebeek FE, Khosrovani S, Witter L, De Zeeuw CI (2008) Purkinje cell input to cerebellar nuclei in tottering: ultrastructure and physiology. Cerebellum 7:547–558.

Hummer A, Delzeith O, Gomez SR, Moreno RL, Mark MD, Herlitze S (2003) Competitive and synergistic interactions of G protein beta(2) and Ca(2+) channel beta(1b) subunits with Ca(v)2.1 channels, revealed by mammalian two-hybrid and fluorescence resonance energy transfer measurements. J Biol Chem 278:49386–49400.

Inchauspe CG, Forsythe ID, Uchitel OD (2007) Changes in synaptic transmission properties due to the expression of N-type calcium channels at the calyx of Held synapse of mice lacking P/Q-type calcium channels. J Physiol 584:835–851.

Iwasaki S, Momiyama A, Uchitel OD, Takahashi T (2000) Developmental changes in calcium channel types mediating central synaptic transmission. J Neurosci 20:59–65.

Jun K, Piedras-Renteria ES, Smith SM, Wheeler DB, Lee SB, Lee TG, Chin H, Adams ME, Scheller RH, Tsien RW, Shin HS (1999) Ablation of P/Q-type Ca(2+) channel currents, altered synaptic transmission, and progressive ataxia in mice lacking the alpha(1A)-subunit. Proc Natl Acad Sci U S A 96:15245–15250.

Khaliq ZM, Raman IM (2006) Relative contributions of axonal and somatic Na channels to action potential initiation in cerebellar Purkinje neurons. J Neurosci 26:1935–1944.

Khan Z, Jinnah HA (2002) Paroxysmal dyskinesias in the lethargic mouse mutant. J Neurosci 22:8193–8200.

Kodama T, Itsukaichi-Nishida Y, Fukazawa Y, Wakamori M, Miyata M, Molnar E, Mori Y, Shigemoto R, Imoto K (2006) A CaV2.1 calcium channel mutation rocker reduces the number of postsynaptic AMPA receptors in parallel fiber-Purkinje cell synapses. Eur J Neurosci 24:2993–3007.

Kordasiewicz HB, Gomez CM (2007) Molecular pathogenesis of spinocerebellar ataxia type 6. Neurotherapeutics 4:285–294.

Levin SI, Khaliq ZM, Aman TK, Grieco TM, Kearney JA, Raman IM, Meisler MH (2006) Impaired motor function in mice with cell-specific knockout of sodium channel Scn8a (NaV1.6) in cerebellar purkinje neurons and granule cells. J Neurophysiol 96:785–793.

Llinas R, Sugimori M (1980a) Electrophysiological properties of in vitro Purkinje cell somata in mammalian cerebellar slices. J Physiol 305:171–195.

Llinas R, Sugimori M (1980b) Electrophysiological properties of in vitro Purkinje cell dendrites in mammalian cerebellar slices. J Physiol 305:197–213.

Llinas R, Sugimori M, Lin JW, Cherksey B (1989) Blocking and isolation of a calcium channel from neurons in mammals and cephalopods utilizing a toxin fraction (FTX) from funnel-web spider poison. Proc Natl Acad Sci U S A 86:1689–1693.

Madisen L, Zwingman TA, Sunkin SM, Oh SW, Zariwala HA, Gu H, Ng LL, Palmiter RD, Hawrylycz MJ, Jones AR, Lein ES, Zeng H (2010) A robust and high-throughput Cre reporting and characterization system for the whole mouse brain. Nat Neurosci 13:133–140.

Mark MD, Liu Y, Wong ST, Hinds TR, Storm DR (1995) Stimulation of neurite outgrowth in PC12 cells by EGF and KCl depolarization: a Ca(2+)-independent phenomenon. J Cell Biol 130:701–710.

Meeren H, van Luijtelaar G, Lopes da Silva F, Coenen A (2005) Evolving concepts on the pathophysiology of absence seizures: the cortical focus theory. Arch Neurol 62:371–376.

Mintz IM, Venema VJ, Swiderek KM, Lee TD, Bean BP, Adams ME (1992a) P-type calcium channels blocked by the spider toxin omega-Aga-IVA. Nature 355:827–829.

Mintz IM, Adams ME, Bean BP (1992b) P-type calcium channels in rat central and peripheral neurons. Neuron 9:85–95.

Mori Y, Wakamori M, Oda S, Fletcher CF, Sekiguchi N, Mori E, Copeland NG, Jenkins NA, Matsushita K, Matsuyama Z, Imoto K (2000) Reduced voltage sensitivity of activation of P/Q-type Ca2+ channels is associated with the ataxic mouse mutation rolling Nagoya (tg(rol)). J Neurosci 20:5654–5662.

Neychev VK, Fan X, Mitev VI, Hess EJ, Jinnah HA (2008) The basal ganglia and cerebellum interact in the expression of dystonic movement. Brain 131:2499–2509.

Noebels JL, Sidman RL (1979) Inherited epilepsy: spike-wave and focal motor seizures in the mutant mouse tottering. Science 204:1334–1336.

Oberdick J, Smeyne RJ, Mann JR, Zackson S, Morgan JI (1990) A promoter that drives transgene expression in cerebellar Purkinje and retinal bipolar neurons. Science 248:223–226.

O'Gorman S, Dagenais NA, Qian M, Marchuk Y (1997) Protamine-Cre recombinase transgenes efficiently recombine target sequences in the male germ line of mice, but not in embryonic stem cells. Proc Natl Acad Sci U S A 94:14602–14607.

Pietrobon D (2005) Function and dysfunction of synaptic calcium channels: insights from mouse models. Curr Opin Neurobiol 15:257–265.

Pietrobon D (2010) CaV2.1 channelopathies. Pflugers Arch 460:375–393.

Pizoli CE, Jinnah HA, Billingsley ML, Hess EJ (2002) Abnormal cerebellar signaling induces dystonia in mice. J Neurosci 22:7825–7833.

Qian J, Noebels JL (2000) Presynaptic Ca(2+) influx at a mouse central synapse with Ca(2+) channel subunit mutations. J Neurosci 20:163–170.

Raman IM, Bean BP (1997) Resurgent sodium current and action potential formation in dissociated cerebellar Purkinje neurons. J Neurosci 17:4517–4526.

Raman IM, Bean BP (1999) Ionic currents underlying spontaneous action potentials in isolated cerebellar Purkinje neurons. J Neurosci 19:1663–1674.

Reid CA, Bekkers JM, Clements JD (2003) Presynaptic Ca2+ channels: a functional patchwork. Trends Neurosci 26:683–687.

Rhyu IJ, Abbott LC, Walker DB, Sotelo C (1999a) An ultrastructural study of granule cell/Purkinje cell synapses in tottering (tg/tg), leaner (tg(la)/tg(la)) and compound heterozygous tottering/leaner (tg/tg(la)) mice. Neuroscience 90:717–728.

Rhyu IJ, Oda S, Uhm CS, Kim H, Suh YS, Abbott LC (1999b) Morphologic investigation of rolling mouse Nagoya (tg(rol)/tg(rol)) cerebellar Purkinje cells: an ataxic mutant, revisited. Neurosci Lett 266:49–52.

Sawada K, Kalam Azad A, Sakata-Haga H, Lee NS, Jeong YG, Fukui Y (2009) Striking pattern of Purkinje cell loss in cerebellum of an ataxic mutant mouse, tottering. Acta Neurobiol Exp (Wars) 69:138–145.

Sohal VS, Huguenard JR (2003) Inhibitory interconnections control burst pattern and emergent network synchrony in reticular thalamus. J Neurosci 23:8978–8988.

Steriade M, Llinas RR (1988) The functional states of the thalamus and the associated neuronal interplay. Physiol Rev 68:649–742.

Strupp M, Zwergal A, Brandt T (2007) Episodic ataxia type 2. Neurotherapeutics 4:267–273.

Swensen AM, Bean BP (2003) Ionic mechanisms of burst firing in dissociated Purkinje neurons. J Neurosci 23:9650–9663.

Tank DW, Sugimori M, Connor JA, Llinas RR (1988) Spatially resolved calcium dynamics of mammalian Purkinje cells in cerebellar slice. Science 242:773–777.

Timofeev I, Steriade M (2004) Neocortical seizures: initiation, development and cessation. Neuroscience 123:299–336.

Todorov B, van de Ven RC, Kaja S, Broos LA, Verbeek SJ, Plomp JJ, Ferrari MD, Frants RR, van den Maagdenberg AM (2006) Conditional inactivation of the Cacna1a gene in transgenic mice. Genesis 44:589–594.

Tybulewicz VL, Crawford CE, Jackson PK, Bronson RT, Mulligan RC (1991)

Neonatal lethality and lymphopenia in mice with a homozygous disruption of the c-abl proto-oncogene. Cell 65:1153–1163.

Walter JT, Alvina K, Womack MD, Chevez C, Khodakhah K (2006) Decreases in the precision of Purkinje cell pacemaking cause cerebellar dysfunction and ataxia. Nat Neurosci 9:389–397.

Womack M, Khodakhah K (2002) Active contribution of dendrites to the tonic and trimodal patterns of activity in cerebellar Purkinje neurons. J Neurosci 22:10603–10612.

Womack MD, Khodakhah K (2003) Somatic and dendritic small-conductance calcium-activated potassium channels regulate the output of cerebellar purkinje neurons. J Neurosci 23:2600–2607.

Womack MD, Khodakhah K (2004) Dendritic control of spontaneous bursting in cerebellar Purkinje cells. J Neurosci 24:3511–3521.

Womack MD, Chevez C, Khodakhah K (2004) Calcium-activated potassium channels are selectively coupled to P/Q-type calcium channels in cerebellar Purkinje neurons. J Neurosci 24:8818–8822.

Wulff P, Schonewille M, Renzi M, Viltono L, Sassoe-Pognetto M, Badura A, Gao Z, Hoebeek FE, van Dorp S, Wisden W, Farrant M, De Zeeuw CI (2009) Synaptic inhibition of Purkinje cells mediates consolidation of vestibulo-cerebellar motor learning. Nat Neurosci 12:1042–1049.

Zhang Y, Vilaythong AP, Yoshor D, Noebels JL (2004) Elevated thalamic low-voltage-activated currents precede the onset of absence epilepsy in the SNAP25-deficient mouse mutant *Coloboma*. J Neurosci 24:5239–5248.

Zwingman TA, Neumann PE, Noebels JL, Herrup K (2001) Rocker is a new variant of the voltage-dependent calcium channel gene Cacna1a. J Neurosci 21:1169–1178.